CBPF

PHD THESIS

Micro-to-macro and Macro-to-micro Quantum Mapping: a Coarse-graining Approach

Student:
Pedro SILVA CORREIA

Advisor:
Dr. Fernando DE MELO
Co-advisor:
Dr. Raul Oscar VALLEJOS

May 17, 2021

CBPF

Abstract

Quantum Information Group - CBPF
COTEO

Micro-to-macro and Macro-to-micro Quantum Mapping: a Coarse-graining Approach

by Pedro SILVA CORREIA

If quantum mechanics is the fundamental theory in physics, at least in principle, it must assign states at every level of description of a system. Consequently, quantum mechanics must provide a two-way of describing nature. Firstly, the theory should connect a microscopic state to a macroscopic (effective) description of a system. Secondly, in an opposite direction, assuming access only to a macroscopic description of a system, quantum mechanics must assign to it an ensemble of microscopic quantum states that abides by all macroscopic constraints. This thesis proposes to investigate both directions, which we named *micro-to-macro* mapping and *macro-to-micro* mapping. We first formalize a coarse-graining map that plays the role of a general *micro-to-macro* mapping. Such an approach aims to model general macroscopic descriptions of a quantum system, even when there is an ambiguity in the split between system's and environment's degrees of freedom. As an application, we construct a coarse-graining map to model an imperfect detection of a well-isolated spin-system in an optical lattice scenario. We readily apply this coarse-graining to describe spin-entanglement dynamics in different ranges of resolution of the system. In the second part of the thesis, assuming that our macroscopic perception of nature is inherently coarse-grained, we construct a *macro-to-micro* operation called averaging assignment map. This map assigns to a set of macroscopic coarse-grained observations a microscopic description which is the ensemble-average of all microscopic states that are compatible with that effective observations. As an application, we construct a nonlinear stochastic state dynamical map that emerges from underlying deterministic linear quantum evolution. As a by-product, we show how effective nonlinear dynamics can be used to improve state discrimination.

Contents

List of Figures

Chapter 1

Introduction

Currently, quantum mechanics plays the role of a fundamental theory of physics. A century has passed since its birth, and quantum mechanics has been proving to be the most successful scientific theory ever formulated. Such status is mainly attributed to the extraordinary agreement between theoretical predictions and the varied experimental results at levels never seen in science. A remarkable example is the prediction for the electron g-factor [1], which has an extraordinary experimental agreement within ten parts in a billion [2]. If today, for instance, matter at its subatomic level is successfully described by the standard model of particles physics [3], it is thanks to its root in quantum mechanics.

Given its fundamental character, quantum mechanics should not be thought of as a theory that deals only with small constituents or larger physical systems at very restricted conditions – as for instance the Bose–Einstein condensate, typically formed when a boson gas at a low density is cooled to extremely low temperatures [4]. Indeed, all the knowledge we have about nature provided by modern science, supports a reductionist view of the laws of nature: the behavior of the parts determines the behavior of the whole. Consequently, as the atomic hypothesis states that the macroscopic world is composed of a collection of small constituents, quantum mechanics directly assumes a universal status. Quantum mechanics predictions, in principle, must then be in agreement with phenomena in all ranges of description.

The universality of quantum mechanics implies a bidirectional way to describe nature.

Firstly, a *micro-to-macro* direction: given a microscopic description of a quantum system, the theory must be able to explain how macroscopic (effective) observations emerge. Secondly, in opposite way, a *macro-to-micro* direction: given a macroscopic observation that effectively describes a system, the theory must assign to it a properly compatible ensemble of microscopic quantum states. Note that what we mean by a macroscopic description of a system is that given by a few effective degrees of freedom, while in a microscopic description we assume a complete characterization of the underlying physical system. In Figure 1.1 we illustrate this bidirectional mapping in a pictorial way.

(a) **Micro-to-macro mapping**

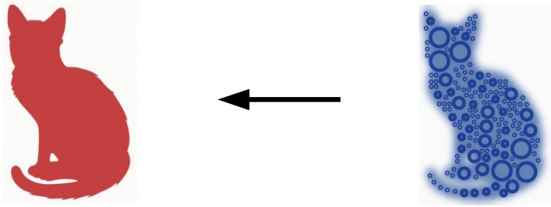

(b) **Macro-to-micro mapping**

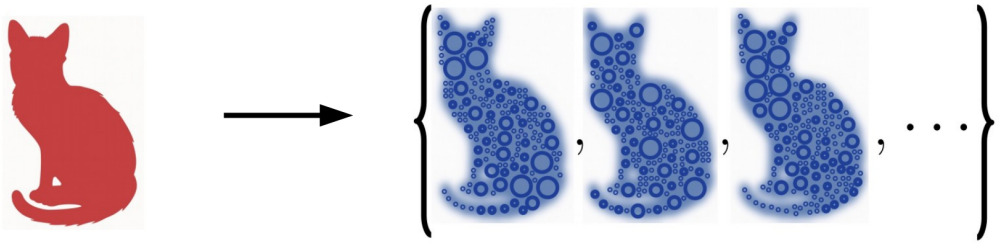

FIGURE 1.1: (a) The **micro-to-macro mapping** assigns to a full microscopically described system a macroscopic (effective) description. A microscopic description of a cat (in blue), that takes into account the state of all its fundamental particles (blue circles in the cat), is mapped to a macroscopic description (red cat). (b) The **micro-to-macro mapping** assigns to a macroscopic description an ensemble of microscopic states that are in agreement with the observed data. Given a macroscopic description of a cat the macro-to-micro map assigns an ensemble of microscopic states that the cat can be in.

The present thesis aims to give a contribution in the generalization of both *micro-to-macro* and *macro-to-micro* assignments. In the following sections we summarize some motivations for the study of both *micro-to-macro* and *macro-to-micro* assignments. We will briefly contextualize some traditional frameworks in which such studies are currently

addressed in the literature, summarizing their domains of application and its limitations. Then it will be succinctly indicated and discussed what will be the main ideas and methodologies adopted in this work for the construction of our approach.

1.1 Micro-to-macro

Throughout the development of quantum physics, a major motivation for the study of micro-to-macro mapping was the attempt to reconcile our everyday perception of nature with intriguing properties of quantum mechanics.

A prominent example is the effort to physically interpret quantum entanglement [5], and why such a fundamental quantum property does not seem to exist in the macroscopic world. Basically, such an issue was guided by the question: "What process does a *microscopic* quantum-described system undergo such that in a *macroscopic* observation entanglement does not seem to exist?".

A traditional approach to deal with this question is based on the *quantum open system paradigm* [6]. Such a scenario acknowledges the fact that no physical system is completely isolated from its surroundings. Therefore, to suitably describe a quantum system, we need to consider its coupling to the surrounding environment – the latter being a "huge" quantum system whose microscopic degrees of freedom are inaccessible. Then, in the open quantum system scenario, the effective description of a system is given by splitting the microscopic degrees of freedom, between those we have access to – identified as the system – from those we don't have access – the environment – which are then removed – See Figure 1.2 (b). Mathematically this removal of environmental variables is given by the partial trace map, through this procedure quantumness seems very sensitive.

Despite being successful in its application regime [6], the open quantum system paradigm has crucial limitations in representing more general effective descriptions. As described above, such an approach is limited to model physical scenarios which present a clear microscopic split between the degrees of freedom of the system and environment, in which

the partial trace can be properly applied. So for general applications, the open quantum system scenario must be generalized.

It is worth to mention that, especially in the scope of the development of quantum technologies, there is a renewed demand for the study of more general *micro-to-macro* mapping. Nowadays, well-isolated quantum systems with a significant number of qubits are at the disposal of physicists [7, 8, 9]. However, its control and characterization consume expensive resources growing with system size. Quantum state tomography, for example, beyond requiring quite accurate individual particle access, in the case of a large system makes its realization and data postprocessing intrinsically time consuming [10]. Therefore, since fundamental quantum features are a crucial resource for the development of quantum technologies – for example, quantum computation and cryptography [11, 12, 13] – it is of fundamental importance an approach that can describe how both the environment and unsharp measurements can affect quantum properties to be detected.

Motivated by these problematic circumstances, in this thesis, we define a general *micro-to-macro* map that aims to overcome some of the limitations presented in the open quantum system paradigm. Supported by the quantum information formalism and its tools, we formalize a *coarse-graining* map that aims to model general situations where we don't have full microscopic access of a quantum system. We pictorially represent in Figure 1.2 (c) an effective (coarse-grained) description of a closed quantum system, which in general cannot be modeled in the open quantum systems approach. Then, employing such a coarse-graining framework, we generalize the open quantum system scenario to an extended definition of subsystems [14, 15, 16, 17].

Once formalized, as a concrete application of our coarse-graining approach, we construct a map that models an imperfect resolution detection of an isolated quantum system [18, 16]. We readily apply such a map to describe the dynamics of spin-entanglement in a coarse-grained optical lattice. Our results suggest that even if we are not able to fully resolve the system, entanglement can still be detected at some coarse-graining levels.

(a) **Microscopic system** (b) **Open quantum system** (c) **Coarse-grained system**

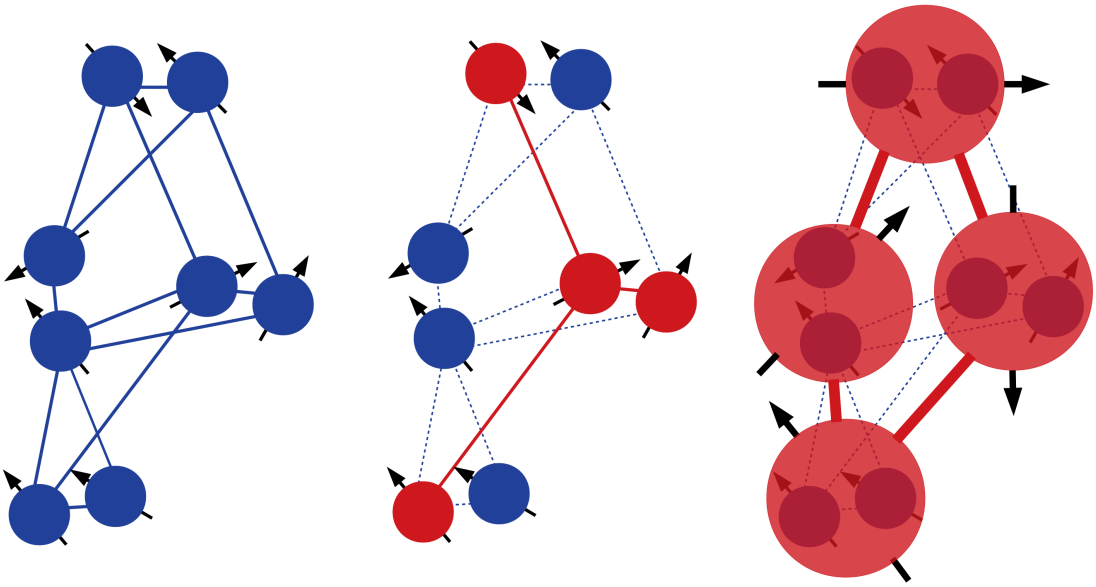

FIGURE 1.2: (a) Here we represent a quantum system composed by a set of qubits (the blue circles with arrow) with the interaction among them represented by blue lines. In a fully microscopic description we must take into account all degrees of freedom (a single qubit represents one local degree of freedom). (b) in the open quantum system scenario the effective description of a system is given by splitting the microscopic degrees of freedom between those we have access to, the red qubits – identified as the system – from those we don't have access to – the environment – which are removed by the partial-trace map. (c) An example of a scenario where, depending on how coarse-grained is the effective description, the open quantum system scenario cannot be applied. In this case the effective description of the underlying microscopic system is given by coarse-grained qubits, each one related to a coarse-grained detection of two qubits. Physically speaking, such a scenario can model a situation where we do not resolve any individual microscopic degree of freedom of the system, but we only have access to the effective description that emerges from a blurry detection of the whole system.

1.2 Macro-to-micro

As stated before, the *macro-to-micro* quantum mapping has the role of assigning a quantum microscopic description that properly represents a given arbitrary set of macroscopic observations. In the literature, such assignments are in general covered by the theory of quantum statistical physics [19, 20]. Traditionally, such an approach also assumes the open quantum system scenario: a "small" system of interest interacting with a "large"

environment (also referred to as reservoir), about which we do not have microscopic control. Considering a set of macroscopic properties about the system and/or its reservoir (e.g. volume, pressure, temperature), statistical physics asserts that the best description of the system, depending on the case, is given by the canonical ensemble. However, now in the macro-to-micro perspective, the quantum open system assumption also comes with the limitations previously pointed.

Therefore, with the intention of formalizing an approach that can describe the diversity of ways that a system can be macroscopically characterized, we formalize a general *macro-to-micro* quantum mapping. Basically, our method assigns to an arbitrary set of macroscopic (coarse-grained) observations, a microscopic ensemble which is the average of all quantum states that the underlying physical system could be in.

Macro-to-micro assignments play an important role in elucidating emergent phenomena in physics [21]. Among its capabilities, this procedure must be able to show how emerging macroscopic behavior is in accordance with the underlying quantum mechanics rules. Emergent nonlinear dynamics, for example, is one of these phenomena that still lacks a general first principle description. Thus, as a by-product of our *macro-to-micro* mapping, we derive a description of general effective stochastic dynamics, which makes more clear under which conditions nonlinear dynamics emerges from linear quantum dynamics. In simple terms, as it will be properly demonstrated, in our approach the nonlinear character will depend not only on how the system microscopically evolves but on how "coarse-grained" is our ability to prepare a physical system.

1.3 Overview

This thesis is organized as follows:

- In Chapter 2, we formalize the micro-to-macro mapping. Grounded on quantum information formalism, we will define a general coarse-graining map that connects a microscopic quantum state of a system to macroscopic/effective descriptions. As

an application, we discuss two coarse-graining maps, the partial trace operation, and a map that models a blurred and saturated detection in an optical lattice scenario.

- In Chapter 3 we explore the blurred and saturated coarse-graining map as a tool to describe spin-entanglement in an optical lattice scenario with different levels of resolution. Comparing it with recent experimental realizations performed with ultracold atoms, we describe to what coarse-grained level the entanglement could still be detected.

- In Chapter 4, we formalize the macro-to-micro mapping. Assuming that we only have a coarse-grained description of a system, we show how to assign to it a microscopic quantum state that abides by all macroscopic constraints. As an application, we construct an effective state dynamics approach, and show how nonlinear dynamics can emerge from linear quantum evolution. We readily apply such nonlinear dynamics to a state discrimination task.

- In Chapter 5, we summarize the leading results of the thesis and make final comments about the most important message we want to convey. We also list applications and perspectives for the continuity of our work.

Chapter 2

Micro-to-macro assignments: Coarse-graining maps

As discussed in the previous chapter, the universality of quantum theory implies a two-way of describing nature: a micro-to-macro and a macro-to-micro. In this chapter, we will propose a model for the former. From a quantum information perspective, we will formalize a coarse-graining map that plays the role of a general micro-to-macro mapping. The main virtue of such coarse-graining formalism is its general character. In principle, such an approach is able to model general (macroscopic) effective descriptions of a quantum system, even when there is an ambiguity in the split between the degrees of freedom of system and environment. As an application, two coarse-graining maps will be discussed, the partial trace operation, and a map that models a blurred and saturated detection in an optical lattice scenario.

The essential idea of coarse-graining models is to provide a description of a complex many-body system focusing only on a small number of effective degrees of freedom. From this basic idea, coarse-grained models are widely used in many branches of science. In chemistry, for instance, it aims to model complex protein structures, dynamics, and interactions [22]. In biology, coarse-graining approaches are used to study how a function of biological structures emerges from molecular-scale dynamics [23]. In computer science, coarse-graining models are also known as granularity models, and are specially used in

parallelism computation techniques [24]. Finally, in physics, coarse-graining models play a crucial role in plenty of different areas. We can highlight, as an example, two seminal coarse-graining approaches, within statistical physics. The first, is the Ehrenfest's coarse-graining procedure, which plays a fundamental role in the seminal work [25], presenting an argument on how irreversibility can be derived from reversible classical dynamics. The second example, we can cite the coarse-graining approach in Kadanoff's blocking procedure [26], which can be considered as the basis of the Wilson renormalization group [27] and modern renormalization group approaches [28].

Given the multiplicity of scenarios and contexts in which coarse-graining models are used, it is to be expected that such models are defined in many different ways. In this work, the coarse-graining framework is constructed in a quantum information context. As it will be described in the next sections, the coarse-graining procedure is defined as a quantum operation [11] which reduces the dimension of a microscopic quantum state, thus resulting in what we called a coarse-grained system.

This chapter is organized as follows, firstly the quantum operation formalism will be presented, in Sec. 2.1. In the sequence, in Sec. 2.2, we will define our general coarse-graining map, finishing with the two important examples that will be used in this thesis: the partial trace map and the blurred and saturated detector map.

2.1 Quantum operations

In quantum mechanics, the quantum operation formalism aims to describe the set of general transformations that a quantum system can undergo. In the context of quantum information, a quantum operation also is usually called a quantum channel.

There are different but equivalent ways of defining quantum operations, here we choose a physically motivated axiomatic approach [11].

Given $\mathcal{L}(\mathcal{H})$ the linear operators acting on $\mathcal{H}$, a quantum map represented by $\mathcal{E}$:

$\mathcal{L}(\mathcal{H}_A) \to \mathcal{L}(\mathcal{H}_B)$, is a quantum operation if it obeys the following three axiomatic properties:

1. Firstly, $\mathcal{E}$ must be trace preserving (TP):

$$\mathrm{tr}\big[\mathcal{E}[M]\big] = \mathrm{tr}[M], \tag{2.1}$$

with M being any linear operator in $\mathcal{L}(\mathcal{H}_A)$.

2. Secondly, the quantum operation $\mathcal{E}$ is a convex-linear map on the set of density operators

$$\mathcal{E}\big[\sum_i p_i\psi_i\big] = \sum_i p_i\mathcal{E}[\psi_i] \tag{2.2}$$

where $\psi_i \in \mathcal{L}(\mathcal{H}_A)$ with probabilities $\{p_i\}$.

3. Thirdly, $\mathcal{E}$ must be completely positive (CP). That is, if $\mathcal{E} : \mathcal{L}(\mathcal{H}_A) \to \mathcal{L}(\mathcal{H}_B)$, then $\mathcal{E}[M] \geq 0$ for any positive operator $M \in \mathcal{L}(\mathcal{H}_A)$. Moreover, if we introduce an extra system E with arbitrary dimension, it must be true that $(\mathcal{E} \otimes \mathbb{1}_E)[M] \geq 0$ for any positive operator $M \in \mathcal{L}(\mathcal{H}_A \otimes \mathcal{H}_E)$, where $\mathbb{1}_E$ denotes the identity map in $\mathcal{H}_E$.

Each of these three axioms represents a particular and important physical property that a quantum operation $\mathcal{E}$ must obey. The first axiom ensures the conservation of the norm: $\mathrm{tr}[\psi] = \mathrm{tr}[\mathcal{E}[\psi]] = 1$.

The second property, comes from the reasonable assumption that a general quantum process $\mathcal{E} : \mathcal{L}(\mathcal{H}_A) \to \mathcal{L}(\mathcal{H}_B)$ must act linearly on mixture of pure state. That is, suppose the input preparation $\psi \in \mathcal{L}(\mathcal{H}_A)$ to $\mathcal{E}$ is acquired by randomly picking a state from an ensemble $\{p_i, \psi_i\}$ of quantum states, so $\psi = \sum_i p_i\psi_i$. Due to the linearity of quantum processes, it is expected that the resulting state $\mathcal{E}[\psi] \in \mathcal{L}(\mathcal{H}_B)$ corresponds to a random selection from the ensemble $\{p(i), \mathcal{E}[\psi_i]\}$, so $\mathcal{E}[\psi] = \sum_i p_i\mathcal{E}[\psi_i]$. Besides,

as demonstrated by Gisin in [29], any deterministic nonlinear quantum operation allows communication in a finite time over arbitrarily large distances, violating the non-signaling principle, then broken the compatibility between quantum mechanics and special theory of relativity.

Finally, the third property also comes as a physical requirement on a quantum operation. Beyond $\mathcal{E}(\psi)$ be a valid density operator, considering as input a bipartite system described by the density operator $\psi_{AE} \in \mathcal{L}(\mathcal{H}_A \otimes \mathcal{H}_E)$, if $\mathcal{E}$ acts only on A, $(\mathcal{E} \otimes \mathbb{1})[\psi_{AE}]$ must still result in a valid state in $\mathcal{L}(\mathcal{H}_B \otimes \mathcal{H}_E)$.

Therefore, the quantum operation can be simply defined as

Definition: *A quantum operation $\mathcal{E} : \mathcal{L}(\mathcal{H}_A) \rightarrow \mathcal{L}(\mathcal{H}_B)$ is a linear and completely positive trace preserving (CPTP) map, for which:*

$$M \rightarrow \mathcal{E}[M] \tag{2.3}$$

for any linear operator $M \in \mathcal{L}(\mathcal{H}_A)$.

As a trivial example, considering a system described by a density operator $\psi \in \mathcal{L}(\mathcal{H}_A)$, any unitary operation U is an admissible quantum operation

$$\psi \rightarrow U\psi U^{\dagger} = \mathcal{U}[\psi], \tag{2.4}$$

in which $\mathcal{U} : \mathcal{L}(\mathcal{H}_A) \rightarrow \mathcal{L}(\mathcal{H}_A)$.

Once properly defined, now we will present a general and suitable way to represent quantum operations: the Kraus operators sum representation (Kraus representation, in an abbreviated form) [11]:

Theorem: *Let $\mathcal{H}_n$ and $\mathcal{H}_m$ be Hilbert spaces with dimensions n and m, $\mathcal{E} : \mathcal{L}(\mathcal{H}_n) \rightarrow$*

$\mathcal{L}(\mathcal{H}_m)$ is CPTP, if and only if, there exists a finite set of linear operators $\{K_i\}_{i=1}^{N\leq nm}$ with $K_i : \mathcal{H}_n \to \mathcal{H}_m$, such that

$$\mathcal{E}[M] = \sum_i^N K_i M K_i^\dagger, \tag{2.5}$$

with

$$\sum_i^N K_i^\dagger K_i = \mathbb{1}_n. \tag{2.6}$$

The elements $\{K_i\}$ are called Kraus operators.

Relation (2.6) fits the trace-preserving property: $\mathrm{tr}[\mathcal{E}[M]] = \mathrm{tr}\big[\sum_i K_i M K_i^\dagger\big] = \mathrm{tr}\big[\sum_i K_i^\dagger K_i M\big] = \mathrm{tr}[M]$.

Observe that if we can write a transformation in the form of equation (2.5) we know for sure that this transformation is completely positive, and consequently it can be related to a quantum operation.

2.2 Coarse-graining map

Finally, the coarse-graining operation can be properly defined. As mentioned, the central idea of coarse-graining models is to give an effective description of a system taking account only a small number of effective degrees of freedom. Thus, in a simple way, a general quantum coarse-graining map can be defined as

Definition: *A linear and completely positive trace preserving (CPTP) map*

$$\Lambda : \mathcal{L}(\mathcal{H}_D) \to \mathcal{L}(\mathcal{H}_d) \tag{2.7}$$

is a coarse-graining map if $\dim(\mathcal{H}_D) > \dim(\mathcal{H}_d)$.

From this general definition, throughout this work we will explore some useful applications of coarse-graining operations. In the sequence we will present two coarse-graining maps that play an important role in this thesis.

2.2.1 Partial trace

A simple and well-known quantum operation is the partial trace, $\mathrm{tr}_E : \mathcal{L}(\mathcal{H}_S \otimes \mathcal{H}_E) \to \mathcal{L}(\mathcal{H}_S)$, which is indeed a coarse-graining operation. The partial trace is defined as follows:

Definition: *The partial trace map* $\mathrm{tr}_E : \mathcal{L}(\mathcal{H}_S \otimes \mathcal{H}_E) \to \mathcal{L}(\mathcal{H}_S)$*, takes density matrices* $\psi_{SE} \in \mathcal{L}(\mathcal{H}_S \otimes \mathcal{H}_E)$ *to density matrices* $\psi_S \in \mathcal{L}(\mathcal{H}_S)$*. It is defined as the linear extension of the mapping*

$$\mathrm{tr}_E : M_S \otimes M_E \to \mathrm{tr}[M_E] M_S \tag{2.8}$$

for any linear operators $M_S \in \mathcal{L}(\mathcal{H}_S)$ *and* $M_E \in \mathcal{L}(\mathcal{H}_E)$*.*

Consider an arbitrary composite system SE, such that we wish to trace out the subsystem E. Let $\{|a_i\rangle\}$ and $\{|b_i\rangle\}$ be orthonormal bases for $\mathcal{H}_S$ and $\mathcal{H}_E$ respectively. Since any arbitrary linear operator $M_{SE} \in \mathcal{L}(\mathcal{H}_S \otimes \mathcal{H}_E)$ can be written as $M_{SE} = \sum_{ijkl} c_{ijkl} |a_i\rangle\langle a_j| \otimes |b_k\rangle\langle b_l|$, the partial trace over a bipartite operator is defined as follows

$$\begin{aligned} \mathrm{tr}_E[M_{SE}] &= \sum_{ijkl} c_{ijkl} \mathrm{tr}[|b_k\rangle\langle b_l|] |a_i\rangle\langle a_j| \\ &= \sum_{ijkl} c_{ijkl} \underbrace{\langle b_l | b_k \rangle}_{\delta_{lk}} |a_i\rangle\langle a_j| \\ &= \sum_{ijk} c_{ijk} |a_i\rangle\langle a_j| \end{aligned} \tag{2.9}$$

which gives a linear operator $M_S \in \mathcal{L}(\mathcal{H}_S)$.

An easy way to classify the partial trace as a quantum operation is finding a valid Kraus representation (2.5). Considering $K_i : \mathcal{H}_{SE} \to \mathcal{H}_S$ defined by $K_i = \mathbb{1}_S \otimes \langle b_i|$, the partial trace can be written in the Kraus form (2.5), therefore the partial trace is a quantum operation.

Finally, since $\dim(\mathcal{H}_{SE}) > \dim(\mathcal{H}_S)$, the partial trace $\mathrm{tr}_E : \mathcal{L}(\mathcal{H}_S \otimes \mathcal{H}_E) \to \mathcal{L}(\mathcal{H}_S)$ can be also classified as a coarse-graining map.

The partial trace is a quantum operation extensively used in literature. The partial trace is a tool commonly used in situations when the interest is to restrict the description of a whole system only to a particular set of localized subsystems – the already discussed open quantum system scenario. An immediate application is found in the decoherence theory, where the description of the loss of information of a quantum system is described in terms of its interaction with an inaccessible/uncontrolled environment [30]. There, the effective description of a system is given by splitting the microscopic degrees of freedom to which we have access – identified as the system – from the rest of degrees of freedom to which we don't have access – the environment. The latter is removed by the partial-trace map.

2.2.2 A blurred and saturated detector

Now we present a coarse-graining map modeling a blurred and saturated detection of a well-closed quantum system realized in a optical lattice scenario [18, 31]. The construction is directly inspired by fluorescence imaging, which is a detection technique present in experimental realizations with cold atoms in optical lattices [32, 33] and in trapped ions [34].

As background scenery, we start by considering as reference the following experimental procedure. Bose-Hubbard spin-systems, realized with cold atoms in an optical

lattice, can be single-site resolved [35, 36] if the experimentalist is equipped with a high-resolution quantum gas microscope [32, 37]. Such a measurement process is based on the fluorescence technique: roughly, the spin chain is illuminated with a laser in such a way that the microscope detects scattered light by atoms in excited states. Given that, in such realizations, each atom encodes a qubit (a spin-$1/2$), the fluorescence imaging is roughly described as follows: each atom stored in the optical lattice is illuminated with a laser in such a way that if light is scattered, the atom was in excited state $|1\rangle$ whereas if no light is scattered, the atom was in non-excited state $|0\rangle$.

From this basic description of a single-site detection, let us consider an adverse scenario. Imagine that we want to measure the light that comes from a number of neighboring atoms in a lattice by fluorescence imaging, but our detecting device does not have enough resolution to identify the light coming from each individual atom. To describe this situation we can construct a coarse-graining model in such way that we take the information of these multiple unresolved signals as effectively coming from one single atom in a coarse-grained level (such situation is pictorially illustrated in Figure 2.1).

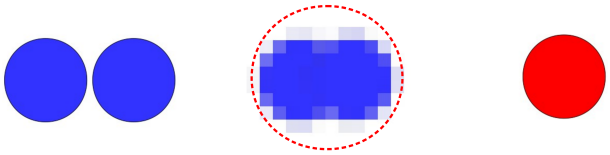

FIGURE 2.1: **A pictorial scheme of coarse-graining model.** In the left the two circles that represent a composite system of two atoms. In the middle we have the blurred detection of the system. Then in the third picture we approximate the blurred signal as a single one related to a single effective atom in a coarse-graining level.

In this way a system of N spins is described by a D-dimensional state $\psi \in \mathcal{L}(\mathcal{H}_D)$, with $D = 2^N$. So we want to construct a coarse-graining map $\Lambda : \mathcal{L}(\mathcal{H}_D) \to \mathcal{L}(\mathcal{H}_2)$ such that it takes a system of N spins to an effective coarse-grained level of a single spin.

Starting from the simplest case, where our detector can not resolve two neighboring atoms and the amount of light coming from a single atom is already sufficient to saturate the detector, the resulting signal can be related to a single atom in a coarse-grained level.

Such situation suggests the following coarse-graining map $\Lambda_{\text{BnS}} : \mathcal{L}(\mathcal{H}_4) \to \mathcal{L}(\mathcal{H}_2)$, introduced in [18, 31]:

$$\begin{array}{l|l}
\Lambda_{\text{BnS}}[|00\rangle\langle 00|] = |0\rangle\langle 0| & \Lambda_{\text{BnS}}[|10\rangle\langle 00|] = \frac{1}{\sqrt{3}}|1\rangle\langle 0| \\
\Lambda_{\text{BnS}}[|00\rangle\langle 01|] = \frac{1}{\sqrt{3}}|0\rangle\langle 1| & \Lambda_{\text{BnS}}[|10\rangle\langle 01|] = 0 \\
\Lambda_{\text{BnS}}[|00\rangle\langle 10|] = \frac{1}{\sqrt{3}}|0\rangle\langle 1| & \Lambda_{\text{BnS}}[|10\rangle\langle 10|] = |1\rangle\langle 1| \\
\Lambda_{\text{BnS}}[|00\rangle\langle 11|] = \frac{1}{\sqrt{3}}|0\rangle\langle 1| & \Lambda_{\text{BnS}}[|10\rangle\langle 11|] = 0 \\
\Lambda_{\text{BnS}}[|01\rangle\langle 00|] = \frac{1}{\sqrt{3}}|1\rangle\langle 0| & \Lambda_{\text{BnS}}[|11\rangle\langle 00|] = \frac{1}{\sqrt{3}}|1\rangle\langle 0| \\
\Lambda_{\text{BnS}}[|01\rangle\langle 01|] = |1\rangle\langle 1| & \Lambda_{\text{BnS}}[|11\rangle\langle 01|] = 0 \\
\Lambda_{\text{BnS}}[|01\rangle\langle 10|] = 0 & \Lambda_{\text{BnS}}[|11\rangle\langle 10|] = 0 \\
\Lambda_{\text{BnS}}[|01\rangle\langle 11|] = 0 & \Lambda_{\text{BnS}}[|11\rangle\langle 11|] = |1\rangle\langle 1|
\end{array} \tag{2.10}$$

The heuristics that lead us to construct such a map are as follows: as the detector cannot resolve if the fluorescence light comes from one atom or the other, then both states $|01\rangle\langle 01|$ and $|10\rangle\langle 10|$ lead to an effective single excitation $|1\rangle\langle 1|$. Moreover, we assume that the detector makes no distinction between one or two excitations, i.e. that it saturates already with a single excitation signal. As such, the state $|11\rangle\langle 11|$ is also mapped to the effective state $|1\rangle\langle 1|$. The coherence between the excited subspace, span$(\{|01\rangle, |10\rangle, |11\rangle\})$, with the no-excitation subspace $|00\rangle$, maps to the effective coherence $1/\sqrt{3}|1\rangle\langle 0|$. The factor $1/\sqrt{3}$ comes from the dimensionality of the subspaces, and it ensures the complete positiveness of the coarse-graining map. Lastly, the coherence terms within the excited subspace, span ($\{|01\rangle$, $|10\rangle$,$|11\rangle\}$), vanish in the coarse-grained description. This occurs because the vectors $|01\rangle$, $|10\rangle$ and $|11\rangle$ cannot be discriminated by the detection process, then no interference between these vectors can be observed in the coarse-grained level.

It is worth to stress the point about the blurred and saturated coarse-graining map Λ_{BnS}, that it cannot be seen as the partial trace tr_E of either one of the two atoms – note in (2.10), that both $|01\rangle\langle 01|$ and $|10\rangle\langle 10|$ are mapped to $|1\rangle\langle 1|$.

To give a better visualization on how such a coarse-graining map transforms a quantum state, consider a general two-qubit pure state $\psi = |\psi\rangle\langle\psi| \in \mathcal{L}(\mathcal{H}_4)$, written in the computational basis: $|\psi\rangle = \sum_{i,j=0}^{1} c_{ij}|ij\rangle$, with $c_{ij} \in \mathbb{C}$ and $\sum_{ij} |c_{ij}|^2 = 1$. Applying the map (2.10), the coarse-grained state is given by:

$$\Lambda_{\mathrm{BnS}}(\psi) = \begin{pmatrix} |c_{00}|^2 & \frac{1}{\sqrt{3}} c_{00}[c_{01}^* + c_{10}^* + c_{11}^*] \\ \frac{1}{\sqrt{3}} c_{00}^*[c_{01} + c_{10} + c_{11}] & |c_{01}|^2 + |c_{10}|^2 + |c_{11}|^2 \end{pmatrix}. \tag{2.11}$$

As stated in the construction of (2.10), here we clearly observe the effective coherences coming from the microscopic states that the blurry detection is able to discriminate, i.e. the coherence between the microscopic excited subspace span($\{|01\rangle, |10\rangle, |11\rangle\}$), with the no-excitation microscopic subspace $|00\rangle$.

The Kraus representation for the blurred and saturated coarse-graining map (2.5) can be easily obtained by a quantum process tomography [11], with the Kraus operators given by:

$$K_1 = \begin{pmatrix} 1 & 0 & 0 & 0 \\ 0 & 1/\sqrt{3} & 1/\sqrt{3} & 1/\sqrt{3} \end{pmatrix} \quad K_3 = \begin{pmatrix} 0 & 0 & 0 & 0 \\ 0 & 1/\sqrt{3} & -1/\sqrt{3} & 0 \end{pmatrix}$$
$$K_2 = \begin{pmatrix} 0 & 0 & 0 & 0 \\ 0 & 1/\sqrt{3} & 0 & -1/\sqrt{3} \end{pmatrix} \quad K_4 = \begin{pmatrix} 0 & 0 & 0 & 0 \\ 0 & 0 & 1/\sqrt{3} & -1/\sqrt{3} \end{pmatrix} \tag{2.12}$$

The blurred and saturated detector $\Lambda_{\mathrm{BnS}} : \mathcal{L}(\mathcal{H}_4) \to \mathcal{L}(\mathcal{H}_2)$ was constructed to model a detector that cannot resolve two neighboring atoms. However, it is of interest to extend such a result in the case where the detector cannot resolve more atoms. As an application, such a extension offers a suitable platform to study the limits of detectability of quantum

features, for example. A straightforward way to do this is by composing Λ_{BnS} as follows:

$$\Lambda_{\mathrm{BnS}}^{4\to1} = \Lambda_{\mathrm{BnS}} \circ (\Lambda_{\mathrm{BnS}} \otimes \Lambda_{\mathrm{BnS}}), \tag{2.13}$$

$$\Lambda_{\mathrm{BnS}}^{8\to1} = \Lambda_{\mathrm{BnS}} \circ (\Lambda_{\mathrm{BnS}} \otimes \Lambda_{\mathrm{BnS}}) \circ \circ (\Lambda_{\mathrm{BnS}} \otimes \Lambda_{\mathrm{BnS}} \otimes \Lambda_{\mathrm{BnS}} \otimes \Lambda_{\mathrm{BnS}}), \tag{2.14}$$

$$\vdots \tag{2.15}$$

$$\Lambda_{\mathrm{BnS}}^{N\to1} = \Lambda_{\mathrm{BnS}} \circ (\Lambda_{\mathrm{BnS}} \otimes \Lambda_{\mathrm{BnS}}) \circ \cdots \circ \circ (\Lambda_{\mathrm{BnS}})^{\otimes\frac{N}{4}} \circ (\Lambda_{\mathrm{BnS}})^{\otimes\frac{N}{2}}, \tag{2.16}$$

the superscript $N \to 1$ indicate that N qubits are mapped to 1, and "$\circ$" denotes composition of maps.

For later convenience, we define the coarse-graining level l as the number of times a layer of coarse-graining maps is applied: for the microscopic level, where no coarse-graining operation is applied we have $l = 0$; starting from N qubits in the microscopic level, a single effective qubit will be obtained at level $l = \log N$ (we use logarithms in base 2 throughout the text) after the application of successive layers of coarse-graining maps. This process is schematically represented in Fig. 2.2.

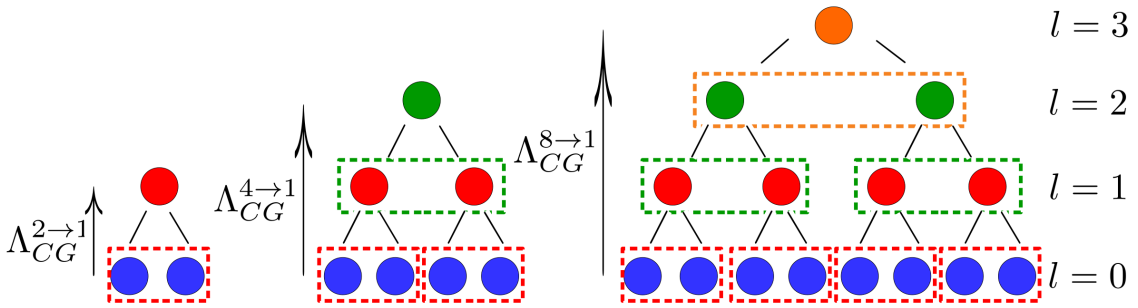

FIGURE 2.2: From a composition of Λ_{BnS}, higher dimensional coarse-graining operations $\Lambda_{\mathrm{BnS}}^{4\to1}$ and $\Lambda_{\mathrm{BnS}}^{8\to1}$ can be defined.

2.3 Summary and conclusions

In this chapter we formalized a general coarse-graining operation $\Lambda : \mathcal{L}(\mathcal{H}_D) \to \mathcal{L}(\mathcal{H}_d)$ that maps a well defined microscopic quantum state $\psi \in \mathcal{L}(\mathcal{H}_D)$ to a coarse-grained state $\varrho \in \mathcal{L}(\mathcal{H}_d)$. The coarse-graining approach generalizes the usual open quantum system scenario, which presumes a clear split between system and environment, to an extended definition of subsystems. As exemplified, in the coarse-graining approach, the loss of information is not related only to the standard open quantum system scenario, in which subsystems that we do not have interest or we are not able to describe are traced out. In the blurred and saturated detection, for instance, the system of interest is the whole system (no subsystem is traced), however the total information we have access to is limited by a lack of resolution in the detector apparatus.

In the next chapters, the analyzed coarse-graining maps will play a central role in two distinct scenarios. Firstly, in Chapter 3, the blurred and saturated detector map will be applied in order to describe spin-entanglement dynamics in different coarse-graining levels of an optical lattice. After that, in Chapter 4, grounded in the premise that macroscopic descriptions are inherently coarse-grained, we will propose a general *macro-to-micro* map which defines the microscopic ensemble that represents general macroscopic observations.

Chapter 3

Entanglement in a coarse-grained optical lattice

Genuine quantum features are no longer exclusively seen as intriguing theoretical predictions of quantum mechanics. Present-day, cutting-edge technologies are intimately dependent on fundamental quantum properties [38]. Besides, such fundamental quantum concepts play a central role as a resource for promising quantum technologies, in special quantum computation and quantum cryptography [11, 12, 13].

However, despite the current stage of technological development allows the exploration of well-isolated quantum systems with an increasing number of qubits [7, 8, 9], crucial difficulties remain. As the size of the system increases, the experimental control and characterization of many-body quantum systems spend expensive resources, making them impracticable. Full quantum state tomography, for instance, requires laborious individual particle access, with both experimental procedure and data post-processing inherently time-consuming for large systems [10].

Given this challenging scenario, effective descriptions may represent a worthwhile alternative to deal with the characterization of quantum many-body systems. Since genuine quantum features may be displayed even in non-completely resolved quantum systems, imprecise (and less costly) measuring processes may then still be useful in characterizing

aspects of quantum many-body systems. Therefore, it is crucial to investigate how different degrees of inaccuracy in a measurement affect the detection of quantum features.

Motivated by the above framework and focusing on entanglement as a genuine quantum feature, in this chapter, we explore the blurred and saturated coarse-graining map (2.10) as a tool to describe spin-entanglement in an optical lattice scenario. It is worth to mention that, since entanglement is fragile in its nature and it is absent in the classical world [39], the study of entanglement decay in a coarse-grained detection, also sheds some light on the quantum-to-classical transition, bringing to the discussion other mechanisms that perturb quantum resources beyond decoherence [39].

This work was inspired by a recent experimental achievement, where many-body entanglement is explored in an ultracold atoms system in an optical lattice [35]. Briefly summarizing, equipped with a high-resolution quantum gas microscope, it was possible to measure spin-entanglement waves in a Bose-Hubbard chain with only a few atoms [35]. Considering this experimental scenario, we explore the blurred and saturated detector map as a tool to analyze up to what coarse-grained level of description entanglement can still be measured. As it will be shown, our results suggest that even if we are not able to fully resolve a system, entanglement can still be detected for some coarse-graining levels. Furthermore, we show that it is possible to have some information about the "microscopic" entanglement, even if we only have access to the system's coarse-grained description. Such a study is the subject of our published paper [40].

This chapter is organized as follows: firstly, in Sec. 3.1, we present a brief description of the entanglement spreading during single spin-impurity dynamics in an one-dimensional Bose-Hubbard system. After that, in Sec. 3.2 we use the blurred and saturated coarse-graining map, defined in Eq. (2.10), to describe the entanglement due to spin-impurity dynamics in a coarse-grained Bose-Hubbard spin-chain. Using concurrence and negativity as entanglement quantifiers, we explore how entanglement behaves taking into account different ranges of resolutions of the spin-chain. Finally in Sec. 3.3 we summarize our results and discuss some implications of this coarse-graining approach.

3.1 Entanglement in a Bose-Hubbard spin-chain

In this section we describe the entanglement generation and spreading during spin-impurity dynamics in a 1D spin-$1/2$ XX-chain [41, 42]. In the mentioned experimental work [35, 36], it was produced a ferromagnetic Heisenberg spin-chain with ultracold bosonic atoms in an optical lattice. In these experiments, individual atoms are trapped in each potential minimum of a periodic potential associated with a stationary wave created by counter-propagating laser beams [43, 44]. Deep in the Mott-insulator regime with unity filling, two hyperfine levels of each atom act as a spin-1/2 (qubit), and neighboring spins interact with each other via isotropic spin-$1/2$ Heisenberg Hamiltonian [45]: $\hat{H} = -J_{ex}\sum_j \vec{\sigma}_j \cdot \vec{\sigma}_{j+1}$. In this Hamiltonian, $\vec{\sigma}_j = (\sigma_{x,j}, \sigma_{y,j}, \sigma_{z,j})$ denotes the spin-$1/2$ vector of Pauli matrices at site j, and J_{ex} is the exchange coupling which is constant for homogeneous chains (see the supplementary information of [36]). In the case of a single spin-impurity in a 1D lattice (single excitation subspace), the Hamiltonian can be written in a simplified form:

$$H = -J_{ex}\sum_j (\sigma_{+,j}\sigma_{-,j+1} + \sigma_{-,j}\sigma_{+,j+1}), \tag{3.1}$$

where $\sigma_{\pm,j} = (\sigma_{x,j} \pm \mathrm{i}\sigma_{y,j})/2$ are the spin-$1/2$ raising (lowering) operators at site j. The term $J_{ex}\sum_j \sigma_{z,j}\sigma_{z,j+1}$ was dropped, since it gives rise only to an energy offset within the single excitation subspace [36].

An infinite spin-up chain with a single spin-down (spin-impurity) on site j can be represented by the state

$$|j\rangle \equiv |\cdots, 0_{j-1}, 1_j, 0_{j+1}, \cdots\rangle, \tag{3.2}$$

where $|1\rangle$ and $|0\rangle$ refer to spin down and spin up states respectively, in the z-basis. As initial state it is considered a single spin-down at the "center" of the chain ($j = 0$). The spin-impurity spreading is given by the time evolution generated by the Hamiltonian in

equation (3.1), and it can be described by

$$|\psi(t)\rangle = \sum_j \phi_j(t)|j\rangle, \tag{3.3}$$

where $\phi_j(t) = i^j J_j(J_{ex}t/\hbar)$, with $J_j(x)$ the Bessel function of the first kind [46]. For simplicity, from now on we will consider the time evolution in dimensionless time unit $J_{ex}t/\hbar$.

3.1.1 Concurrence between two sites

The next step is to quantify the entanglement between spins in two different sites A and B in the chain. The reduced density operator related to a pair of different arbitrary sites A and B is given by:

$$\psi_{AB}(t) = \mathrm{tr}_{\overline{AB}}[|\psi(t)\rangle\langle\psi(t)|], \tag{3.4}$$

where $\overline{AB}$ means the complementary sites to AB. Using (3.3) and the basis states $|00\rangle$, $|01\rangle$, $|10\rangle$ and $|11\rangle$ for sites A and B, we get:

$$\psi_{AB} = \begin{pmatrix} 1-|\phi_A|^2-|\phi_B|^2 & 0 & 0 & 0 \\ 0 & |\phi_B|^2 & \phi_A\phi_B^* & 0 \\ 0 & \phi_A^*\phi_B & |\phi_A|^2 & 0 \\ 0 & 0 & 0 & 0 \end{pmatrix}. \tag{3.5}$$

Explicit time dependence is suppressed whenever obvious, to avoid cluttered notation.

The matrix representation (3.5) of ψ_{AB} can be identified as a X-matrix:

$$X = \begin{pmatrix} X_{11} & 0 & 0 & X_{14} \\ 0 & X_{22} & X_{23} & 0 \\ 0 & X_{23}^* & X_{33} & 0 \\ X_{14}^* & 0 & 0 & X_{44} \end{pmatrix}, \tag{3.6}$$

whose concurrence is easily calculated [47]

$$\mathcal{C}(X) = 2\,\max\{0, |X_{14}| - \sqrt{X_{22}X_{33}}, |X_{23}| - \sqrt{X_{11}X_{44}}\}. \tag{3.7}$$

Thus, the concurrence $\mathcal{C}(\psi_{AB})$ between A and B sites is given by:

$$\mathcal{C}(\psi_{AB}) = 2|\phi_A\phi_B^*|. \tag{3.8}$$

Figure 3.1 illustrates the expected entanglement dynamics between symmetric sites with respect to the spin at position $j = 0$. Such an entanglement wave – see Fig. 3.1(b) – was observed experimentally showing a reasonable agreement with the theoretical prediction [35].

3.2 Entanglement spreading in a CG Spin Chain

Now that we have already constructed the coarse graining map that plays the role of a blurred detector, Eq. (2.10), let's analyze how entanglement evolves under this coarse graining view. In the same way as the entanglement detection was studied in [35], we will calculate the entanglement behavior between two symmetric sites around the center of a spin-chain, but now considering coarse-grained sites, that is, entanglement between two coarse-grained blocks of spins.

Before we start, in order to properly write the microscopic ($l = 0$) reduced state $\psi_{AB}^{l=0}$ on the blocks $A = \{A_1, \ldots, A_N\}$ and $B = \{B_1, \ldots, B_N\}$, it is convenient to define the following family of vectors:

$$\begin{aligned} |k_N\rangle_A &\equiv |0_{A_1}, \cdots, 0_{A_{k-1}}, 1_{A_k}, 0_{A_{k+1}} \cdots, 0_{A_N}\rangle, \\ |0_N\rangle_A &\equiv |0_{A_1}, \cdots, 0_{A_N}\rangle, h \end{aligned} \tag{3.9}$$

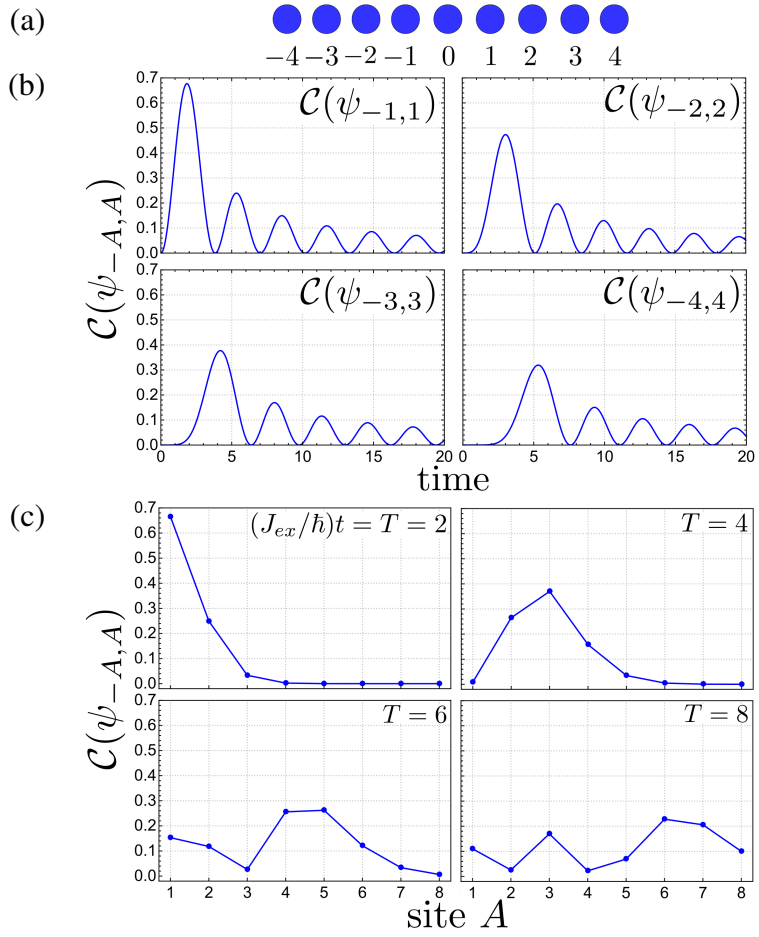

FIGURE 3.1: **Entanglement dynamics of a single impurity spin-chain.** (a) Schematic representation of the spin-chain with its labels. (b) Time evolution of concurrence $\mathcal{C}(\psi_{A,-A})$ between spins of sites A and $-A$ for different choices of A (the time evolution is given in dimensionless unit $J_{ex}t/\hbar$). (c) Spin entanglement wave with single site resolution.

with $k \in \{1, \dots N\}$, and similarly for B. It is clear that $|k_N\rangle_{A(B)}$ is a state vector with a single spin impurity at the k-th site of block $A(B)$, and $|0_N\rangle_{A(B)}$ is the no-impurity state.

3.2.1 $l = 1$: CG Entanglement $(2 \to 1)$

In the first situation, $l = 1$, we want to compute the entanglement between two coarse-grained sites, each one coming from a block of two neighboring sites ($N = 2$) at the microscopic level ($l = 0$), $A = \{A_1, A_2\}$ and $B = \{B_1, B_2\}$, as it is schematically represented in Fig. 3.2. Remembering that we are in the single excitation subspace, and

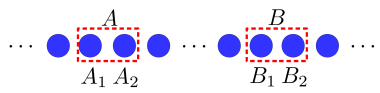

FIGURE 3.2: Schematic representation of a block of spins where the coarse graining map Λ_{BnS} is going to be applied.

using $\{|k_2\rangle_{A(B)}\} \cup |0_2\rangle_{A(B)}$ as basis, the reduced state $\psi_{AB}^{l=0}$ can be written as

$$\begin{aligned}
\psi_{AB}^{l=0} &= \text{tr}_{\overline{AB}}[|\psi(t)\rangle\langle\psi(t)|] \\
&= \big(1 - \sum_{k=1}^{2} |\phi_{A_k}|^2 - \sum_{k=1}^{2} |\phi_{B_k}|^2\big)|0_2\rangle_A\langle 0_2| \otimes |0_2\rangle_B\langle 0_2| + \\
&+ \sum_{k=1}^{2} (|\phi_{A_k}|^2 |k_2\rangle_A\langle k_2| \otimes |0_2\rangle_B\langle 0_2| + |\phi_{B_k}|^2 |0_2\rangle_A\langle 0_2| \otimes |k_2\rangle_B\langle k_2|) + \\
&+ \sum_{k\neq k'=1}^{2} \big(\phi_{A_k}\phi_{A_{k'}}^* |k_2\rangle_A\langle k_2'| \otimes |0_2\rangle_B\langle 0_2| + \phi_{B_k}\phi_{B_{k'}}^* |0_2\rangle_A\langle 0_2| \otimes |k_2\rangle_B\langle k_2'|\big) + \\
&+ \sum_{k,k'=1}^{2} \big(\phi_{A_k}\phi_{B_{k'}}^* |k_2\rangle_A\langle 0_2| \otimes |0_2\rangle_B\langle k_2'| + \phi_{A_k}^*\phi_{B_{k'}} |0_2\rangle_A\langle k_2| \otimes |k_2'\rangle_B\langle 0_2|\big), \qquad (3.10)
\end{aligned}$$

with $|\psi(t)\rangle$ given by Eq. (3.3).

In this form, Eq. (3.10), it is now simple to apply the coarse graining map defined in (2.10). Observe that the internal coherences $\phi_{A_k}\phi_{A_{k'}}^*$ and $\phi_{B_k}\phi_{B_{k'}}^*$ (for $k\neq k'$) related to each spin-block present in state (3.10) no longer survive in the coarse-grained state, as $\Lambda_{\text{BnS}}[|10\rangle\langle 01|] = \Lambda_{\text{BnS}}[|01\rangle\langle 10|] = 0$. The effective two-qubit is then:

$$\begin{aligned}
\psi_{AB}^{l=1} &= (\Lambda_{\text{BnS}} \otimes \Lambda_{\text{BnS}})[\psi_{AB}^{l=0}] \\
&= \begin{pmatrix}
1 - \sum_{k=1}^{2} |\phi_{A_k}|^2 - \sum_{k=1}^{2} |\phi_{B_k}|^2 & 0 & 0 & 0 \\
0 & \sum_{k=1}^{2} |\phi_{B_k}|^2 & \frac{1}{3}\sum_{k,k'=1}^{2} \phi_{A_k}\phi_{B_{k'}}^* & 0 \\
0 & \frac{1}{3}\sum_{k,k'=1}^{2} \phi_{A_k}^*\phi_{B_{k'}} & \sum_{k=1}^{2} |\phi_{A_k}|^2 & 0 \\
0 & 0 & 0 & 0
\end{pmatrix},
\end{aligned} \qquad (3.11)$$

where we used the basis states $\{|k_1\rangle_{A(B)}\} \cup |0_1\rangle_{A(B)}$, for each effective site.

The entanglement between two coarse-grained sites is derived analogously to that found before for two (non-coarse-grained) sites in (3.8). Since the state (3.11) takes the X-form (3.6), using the equation (3.7), its concurrence is given by

$$\mathcal{C}(\psi_{AB}^{l=1}) = \frac{2}{3}\left| \sum_{k,k'=1}^{2} \phi_{A_k}\phi_{B_{k'}}^{*} \right|. \tag{3.12}$$

For the purpose of giving a concrete view of the consequences of this result, we numerically investigated the entanglement evolution in a seventeen sites chain with the spin-impurity beginning at its center. In Fig. 3.3(a) we plot in blue the concurrence between symmetric sites around the center of the spin-chain in the "microscopic" level, and in red the concurrence considering their related coarse-grained sites. In the microscopic level we use Eq. (3.8) to calculate the concurrence between the first two pairs of sites before the coarse graining: $\mathcal{C}(\psi_{1,-1}^{l=0}) = 2|\phi_1\phi_{-1}^{*}|$ and $\mathcal{C}(\psi_{2-2}^{l=0}) = 2|\phi_2\phi_{-2}^{*}|$. Then, we calculate the concurrence of the resulting pair of coarse-grained sites using Eq. (3.12): $\mathcal{C}(\psi_{1,-1}^{l=1}) = (2/3)|(\phi_1 + \phi_2)(\phi_{-1} + \phi_{-2})^{*}|$. In the same way we calculate the concurrence between other symmetric sites around the center both at the microscopic level and at coarse-grained level with $l = 1$.

As expected, we observe that concurrence decays in the coarse graining level. Despite of this, a significant amount of entanglement still survives. Even in the coarse-grained description we observe a propagating entanglement “wave” (See Fig. 3.3(b)), with values above the error bar (black dashed line) coming from the single site detection scenario observed by the experimental realization in [35]. It is interesting to notice that the maximum value of concurrence values in coarse graining level $l = 1$ are in better agreement with the experimental results showed in [35] than when compared with the theoretical results in microscopic level $l = 0$. One can thus speculate that the experimental procedure in [35] does take into account some coarse graining as the one introduced here.

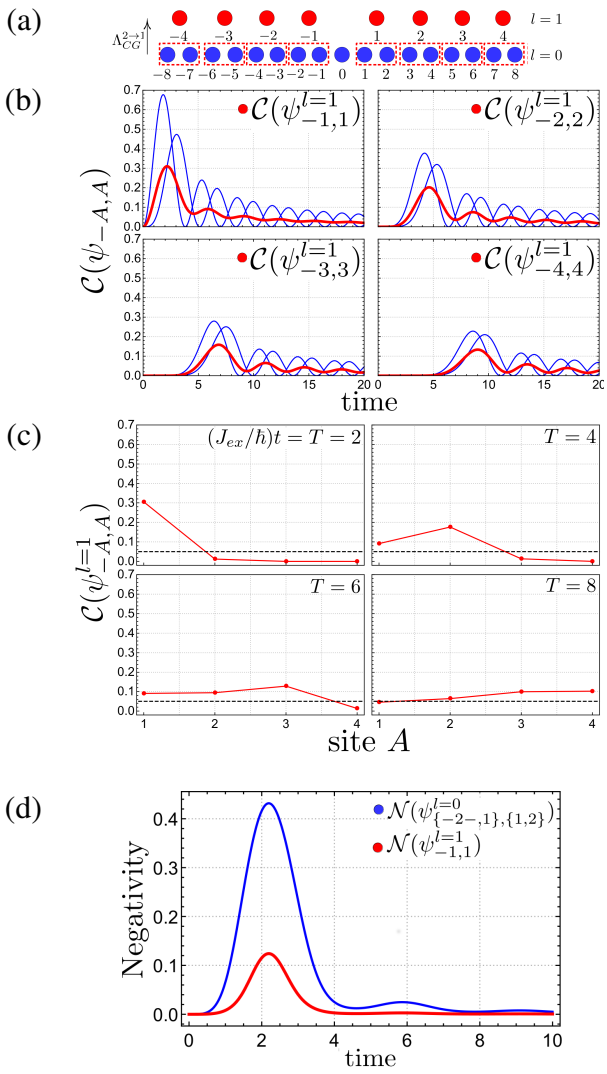

FIGURE 3.3: **Coarse-grained entanglement in $l = 1$.** (a) Effective spin chain with a single layer of coarse graining. (b) Comparison between concurrence evolution of the first four symmetric pairs of coarse-grained sites, $\mathcal{C}(\psi^{l=0}_{-A,A})$ (red line), with respect to the concurrence between their relative pair of microscopic sites (blue lines). (c) Entanglement wave in the coarse-grained level. The black dashed constant line represents the error in experimental detection (taken from [35]). (d) Comparison between negativity evolution of the first symmetric pairs of coarse-grained sites, $\mathcal{N}(\psi^{l=1}_{-1,1})$ (red line), and the negativity $\mathcal{N}(\psi^{l=0}_{\{-2,-1\},\{1,2\}})$ among their relative four microscopic sites (blue lines). The time evolution is given in dimensionless unit $J_{ex}t/\hbar$.

A complementary way of studying the differences in entanglement between the microscopic level and the coarse-grained level is through negativity [48]. Using concurrence we are somewhat restricted to calculate only bipartite entanglement for systems with two

spins (two sites in the spin-chain). Negativity, on the other hand, can be evaluated for bipartite systems of any local dimensions, and it is defined as follows:

$$\mathcal{N}(\psi) = \frac{||\psi^{T_B}||_1 - 1}{2} \tag{3.13}$$

where ψ^{T_B} is the partial transpose of ψ with respect to subsystem B and $||A||_1 = tr\sqrt{(A)^\dagger A}$ is the trace norm.

Here we restrict our analysis to the coarse-grained state $\psi^{l=1}_{-1,1}$ and its related microscopic state $\psi^{l=0}_{\{-2,-1\},\{1,2\}}$. Results are shown in Fig.3.3 (d). Differently from the concurrence approach, with negativity we can properly compare the entanglement within blocks in different ranges of description. We observe that entanglement in the coarse graining level is smaller than the *total* entanglement in the microscopic state.

3.2.2 $l = 2$: CG Entanglement $(4 \to 1)$

For the next level of resolution ($l = 2$), we map four sites ($N = 4$) as a single effective one. Given an arbitrary pair of spin-blocks composed by four neighboring atoms $A = \{A_4, A_3, A_2, A_1\}$ and $B = \{B_1, B_2, B_3, B_4\}$– as shown in Fig. 3.4 – we proceed in the same way as above to find the coarse-grained state.

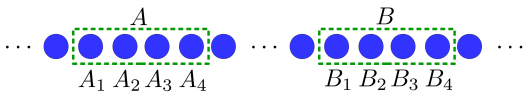

FIGURE 3.4: Schematic representation of a block of spins where the coarse graining map $\Lambda^{4\to1}_{\text{BnS}}$ is going to be applied.

Considering the single excitation subspace, and using $\{|k_4\rangle_{A(B)}\} \cup |0_4\rangle_{A(B)}$ as basis, in this case the reduced state $\psi_{AB}^{l=0}$ where $\Lambda_{\text{BnS}}^{4\to1} \otimes \Lambda_{\text{BnS}}^{4\to1}$ will be applied, can be written as

$$\begin{aligned}
\psi_{AB}^{l=0} &= \text{tr}_{\overline{AB}}[|\psi(t)\rangle\langle\psi(t)|] \\
&= \big(1 - \sum_{k=1}^{4} |\phi_{A_k}|^4 - \sum_{k=1}^{4} |\phi_{B_k}|^4\big)|0_4\rangle_A\langle 0_4| \otimes |0_4\rangle_B\langle 0_4| + \\
&+ \sum_{k=1}^{4}(|\phi_{A_k}|^4 |k_4\rangle_A\langle k_4| \otimes |0_4\rangle_B\langle 0_4| + |\phi_{B_k}|^4 |0_4\rangle_A\langle 0_4| \otimes |k_4\rangle_B\langle k_4|) + \\
&+ \sum_{k\neq k'=1}^{4} \big(\phi_{A_k}\phi_{A_{k'}}^* |k_4\rangle_A\langle k_4'| \otimes |0_4\rangle_B\langle 0_4| + \phi_{B_k}\phi_{B_{k'}}^* |0_4\rangle_A\langle 0_4| \otimes |k_4\rangle_B\langle k_4'|\big) + \\
&+ \sum_{k,k'=1}^{4} \big(\phi_{A_k}\phi_{B_{k'}}^* |k_4\rangle_A\langle 0_4| \otimes |0_4\rangle_B\langle k_4'| + \phi_{A_k}^*\phi_{B_{k'}} |0_4\rangle_A\langle k_4| \otimes |k_4'\rangle_B\langle 0_4|\big), \qquad (3.14)
\end{aligned}$$

with $|\psi(t)\rangle$ given by Eq. (3.3).

Applying $\Lambda_{\text{BnS}}^{4\to1} \otimes \Lambda_{\text{BnS}}^{4\to1}$:

$$\begin{aligned}
\psi_{AB}^{l=2} &= (\Lambda_{\text{BnS}}^{4\to1} \otimes \Lambda_{\text{BnS}}^{4\to1})[\psi_{AB}^{l=0}] \\
&= \begin{pmatrix}
1 - \sum_{k=1}^{4} |\phi_{A_k}|^4 - \sum_{k=1}^{4} |\phi_{B_k}|^2 & 0 & 0 & 0 \\
0 & \sum_{k=1}^{4} |\phi_{B_k}|^2 & \frac{1}{3^2}\sum_{k,k'=1}^{4} \phi_{A_k}\phi_{B_{k'}}^* & 0 \\
0 & \frac{1}{3^2}\sum_{k,k'=1}^{4} \phi_{A_k}^*\phi_{B_{k'}} & \sum_{k=1}^{4} |\phi_{A_k}|^2 & 0 \\
0 & 0 & 0 & 0
\end{pmatrix}. \qquad (3.15)
\end{aligned}$$

As observed in the previous subsection (3.2.1), the internal coherence related to spin-blocks, $\phi_{A_k}\phi_{A_{k'}}^*$ and $\phi_{B_k}\phi_{B_{k'}}^*$, with $k \neq k'$, do not survive in the effective state (3.15). As before, this happens because $\Lambda_{\text{BnS}}[|10\rangle\langle 01|] = \Lambda_{\text{BnS}}[|01\rangle\langle 10|] = 0$, and due to the fact that $\Lambda_{CG}^{4\to1} = \Lambda_{\text{BnS}} \circ (\Lambda_{\text{BnS}} \otimes \Lambda_{\text{BnS}})$. The square power on the $1/3$ factor reflects the two layers of coarse graining which were applied.

For such a state the concurrence can be easily evaluated to give:

$$\mathcal{C}(\psi_{AB}^{l=2}) = \frac{2}{3^2}\left|\sum_{k,k'=1}^{4} 2\phi_{A_k}\phi_{B_{k'}}^{*}\right|. \tag{3.16}$$

Again we analyze the entanglement evolution by looking at the seventeen centralized sites of the microscopic chain ($l = 0$) whose spin-impurity begins at its center. Results are shown in Fig.3.5. We use equation (3.8) to calculate the concurrence between the first four pair of sites before the coarse graining (in blue): $\mathcal{C}(\psi_{-1,1}^{l=0}) = 2|\phi_{-1}\phi_{1}^{*}|$, $\mathcal{C}(\psi_{-2,2}^{l=0}) = 2|\phi_{-2}\phi_{2}^{*}|$, $\mathcal{C}(\psi_{-2,3}^{l=0}) = 2|\phi_{-3}\phi_{3}^{*}|$ and $\mathcal{C}(\psi_{-4,4}^{l=0}) = 2|\phi_{-4}\phi_{4}^{*}|$. Then, we calculate the concurrence of resulting pair of coarse-grained sites using the equation (3.16) (in green): $\mathcal{C}(\psi_{-1,1}^{l=2}) = (2/9)|(\phi_{-1}+\phi_{-2}+\phi_{-3}+\phi_{-4})(\phi_{1}+\phi_{2}+\phi_{3}+\phi_{4})^{*}|$. We proceed in the same way to calculate the concurrence between the other symmetric sites.

As expected, we observe that the concurrence becomes weaker when compared to the concurrence in the microscopic level or even with the one in the first coarse grained level (3.3). Consequently we observe a very weak entanglement "wave", in the limit of the experimental error detection (see 3.3(c)). Therefore in this scheme, if we consider the error bars of the experimental work [35], our results suggest that entanglement would no longer be detectable.

Analogously to the last subsection, here we calculate the negativity for the different description levels of the system $l = 0, 1, 2$. We consider the coarse-grained states $\psi_{-1,1}^{l=2}$ and $\psi_{\{-2,-1\},\{1,2\}}^{l=1}$, and their correspondent microscopic state $\psi_{\{-4,-3,-2,-1\},\{1,2,3,4\}}^{l=0}$. Results are shown in Fig. 3.5 (c). We observe how drastic it is the effect of the coarse graining on the entanglement among different levels. This result is in agreement with the ones for concurrence, indicating a weak entanglement signal after two layers of coarse graining (level $l = 2$). That is, if the detector cannot resolve the signal coming for a ensemble of four neighboring sites in a spin-chain, entanglement will be hardly detectable in the experimental situation. Again we observe that the effective entanglement is smaller than the total entanglement in the super-cell.

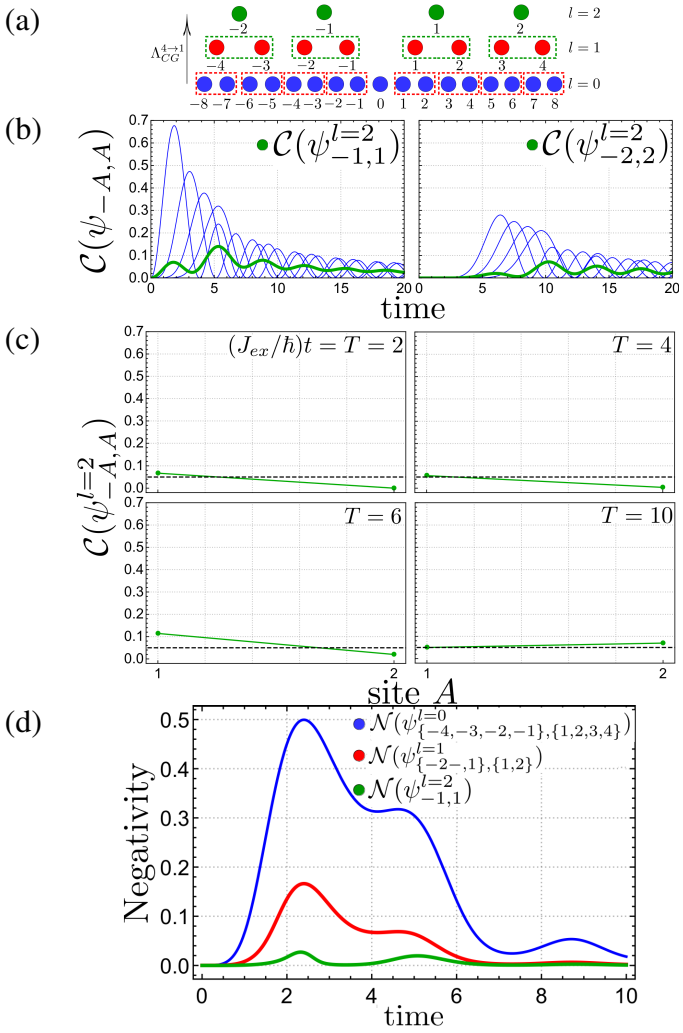

FIGURE 3.5: **Coarse-grained entanglement in $l = 2$.** (a) Effective spin-chain with two layers of coarse graining. (b) Comparison between concurrence evolution of the first two symmetric pairs of coarse-grained sites, $\mathcal{C}(\psi^{l=2}_{-A,A})$ (green line), and the concurrence between their relative eight microscopic sites (blue lines). The time evolution is given in dimensionless unit $J_{ex}t/\hbar$ (c) Spatial dynamics of concurrence in the CG level. The black dashed constant line represents the error in experimental detection. (d) Comparison between negativity evolution in different levels of description, $l = 1$ (upper red line), $l = 2$ (lower green line), and the negativity in the microscopic supercell, $l = 0$ (blue line). The time evolution is given in dimensionless unit $J_{ex}t/\hbar$.

3.2.3 $l = \log N$: CG Entanglement ($N \to 1$)

In this section we generalize the previous concurrence results to any level of coarse graining. At the microscopic level, we consider two blocks of sites $A = \{A_1, A_2, \cdots, A_N\}$ and $B = \{B_1, B_2, \cdots, B_N\}$, in which we will apply $\log N$ layers of the coarse graining

map:

$$\Lambda_{\text{BnS}}^{N\to 1} = \Lambda_{\text{BnS}} \circ (\Lambda_{\text{BnS}} \otimes \Lambda_{\text{BnS}}) \circ \cdots \circ \\ \circ \left(\Lambda_{\text{BnS}}\right)^{\otimes \frac{N}{4}} \circ \left(\Lambda_{\text{BnS}}\right)^{\otimes \frac{N}{2}}. \tag{3.17}$$

Using the total pure state in equation (3.3), and definition (3.9), we can write the reduced state over the blocks A and B as:

$$\begin{aligned}
\psi_{AB}^{l=0} &= \text{tr}_{\overline{AB}}[|\psi(t)\rangle\langle\psi(t)|] \\
&= \big(1 - \sum_{k=1}^{N} |\phi_{A_k}|^2 - \sum_{k=1}^{N} |\phi_{B_k}|^2\big)|0_2\rangle_A\langle 0_2| \otimes |0_2\rangle_B\langle 0_2| + \\
&+ \sum_{k=1}^{N} (|\phi_{A_k}|^2 |k_N\rangle_A\langle k_N| \otimes |0_N\rangle_B\langle 0_N| + |\phi_{B_k}|^2 |0_N\rangle_A\langle 0_N| \otimes |k_N\rangle_B\langle k_N|) + \\
&+ \sum_{k\neq k'=1}^{N} \big(\phi_{A_k}\phi_{A_{k'}}^* |k_N\rangle_A\langle k'_N| \otimes |0_N\rangle_B\langle 0_N| + \phi_{B_k}\phi_{B_{k'}}^* |0_N\rangle_A\langle 0_N| \otimes |k_N\rangle_B\langle k'_N|\big) + \\
&+ \sum_{k,k'=1}^{N} \big(\phi_{A_k}\phi_{B_{k'}}^* |k_N\rangle_A\langle 0_N| \otimes |0_N\rangle_B\langle k'_N| + \phi_{A_k}^*\phi_{B_{k'}} |0_N\rangle_A\langle k_N| \otimes |k'_N\rangle_B\langle 0_N|\big).
\end{aligned} \tag{3.18}$$

The rational to apply the coarse graining map in both supercells, $\Lambda_{CG}^{N\to 1} \otimes \Lambda_{CG}^{N\to 1}$, is as before. The first term contains no excitations, and as such goes to $(1 - \sum_{k=1}^{N} |\phi_{A_k}|^2 - \sum_{k=1}^{N} |\phi_{B_k}|^2)|0\rangle_A\langle 0| \otimes |0\rangle_B\langle 0|$. The second term contains the diagonal/population elements where the excitation is either in part A or in part B. As the coarse graining maps states in the single-excitation subspace into (smaller dimensional) single-excitation subspace, this term goes to $\sum_{k=1}^{N}(|\phi_{A_k}|^2|1\rangle_A\langle 1| \otimes |0\rangle_B\langle 0| + |\phi_{B_k}|^2|0\rangle_A\langle 0| \otimes |1\rangle_B\langle 1|)$. The third term contains off-diagonal/coherence elements where the excitation is either in the part A or in the part B. As $k \neq k'$, these elements represent coherences between states that the detector cannot distinguish, and as such, at some level, these elements vanish. Lastly we have the term

with coherences between the single-excitation subspace and the no-excitation subspace within a supercell. At a given layer there will always be per block one element of the form $|01\rangle_A\langle 00|$ or $|10\rangle_A\langle 00|$, with all others being as $|00\rangle_A\langle 00|$. The action of the coarse graining map on the first type of elements gives $|1\rangle_A\langle 0|/\sqrt{3}$, while on the second gives $|0\rangle_A\langle 0|$. The same reasoning applies for the Hermitian conjugate elements and for the block B. Since we start with N spins per block, we can repeat this process $\log N$ times, and as such, at level $l = \log N$, this term goes to $(1/3)^{\log N}\sum_{k,k'=1}^{N}\phi_{A_k}\phi^*_{B_{k'}}|1\rangle_A\langle 0| \otimes |0\rangle_B\langle 1| + \phi^*_{A_k}\phi_{B_{k'}}|0\rangle_A\langle 1| \otimes |1\rangle_B\langle 0|$. In summary, after applying the coarse graining map $\log N$ times on the pure state (3.3), we get:

$$\psi_{AB}^{l=\log N} = (\Lambda_{CG}^{N\to 1}\otimes\Lambda_{CG}^{N\to 1})[\psi_{AB}^{l=0}]$$
$$= \begin{pmatrix} 1-\sum_{k=1}^{N}|\phi_{A_k}|^2-\sum_{k=1}^{N}|\phi_{B_k}|^2 & 0 & 0 & 0 \\ 0 & \sum_{k=1}^{N}|\phi_{B_k}|^2 & \frac{1}{3^{\log N}}\sum_{k,k'=1}^{N}\phi_{A_k}\phi^*_{B_{k'}} & 0 \\ 0 & \frac{1}{3^{\log N}}\sum_{k,k'=1}^{N}\phi^*_{A_k}\phi_{B_{k'}} & \sum_{k=1}^{N}|\phi_{A_k}|^2 & 0 \\ 0 & 0 & 0 & 0 \end{pmatrix}. \tag{3.19}$$

As before, now it is simple to evaluate the effective concurrence:

$$\mathcal{C}(\psi_{AB}^{l=\log N}) = \frac{2}{3^{\log N}}\Big|\sum_{k,k'=1}^{N}\phi_{A_k}\phi^*_{B_{k'}}\Big|. \tag{3.20}$$

Now we can evaluate the limit of effective concurrence detection. To do this we compare the maximum value attained for concurrence $\mathcal{C}(\psi^l_{-1,1})$ at each coarse graining level. Results are shown in Fig. 3.6. We note that from $l = 3$ onward the values became smaller than the experimental detection error observed in [35], which suggests that no entanglement could be detected in this experimental resolution.

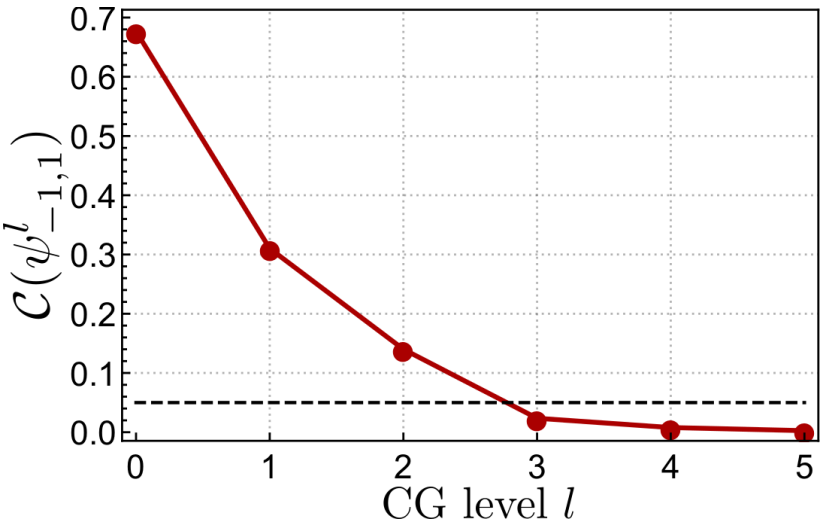

FIGURE 3.6: **Concurrence behavior at each coarse graining level.** Each dot represents the maximum value attained for the concurrence at the respective coarse graining level. The black dashed constant line represents the error in experimental detection.

From Eq. (3.20) it is simple to established that the effective concurrence at a given coarse graining level l is smaller than the sum of all bipartite microscopic concurrences:

$$\mathcal{C}(\psi_{AB}^{l=\log N}) \leq \frac{1}{3^{\log N}} \sum_{k,k'=1}^{N} \mathcal{C}(\psi_{A_k B_{k'}}^{l=0}). \tag{3.21}$$

We observe an exponential entanglement decay with respect to the coarse graining level $l = \log N$.

Moreover, now we can address the following physically motivated question: From the coarse-grained concurrence can we say something about entanglement at the microscopic level? Let

$$\mathcal{C}_{\max}^{l=0} = \max_{k,k'} \mathcal{C}(\psi_{A_k B_{k'}}^{l=0}) \tag{3.22}$$

Then from the above inequality we have:

$$\mathcal{C}_{\max}^{l=0} \geq \left(\frac{3}{4}\right)^{\log N} \mathcal{C}(\psi_{AB}^{l=\log N}). \tag{3.23}$$

Therefore with this procedure we can construct a lower bound for the maximal concurrence between a pair of spins in the microscopic level. Naturally, we are not able to identify the pair of spins which shares the maximum entanglement at a given time, but we can say that there is a pair of spins in the microscopic chain with entanglement at least $(3/4)^{\log N}$ of the concurrence measured in the macroscopic level.

3.3 Summary and conclusions

In the present chapter, we have presented the results related to our paper Ref. [16]. So we explored the blurred and saturated coarse-graining map (2.10), defined in the last chapter, as a tool to describe entanglement dynamics in different degrees of resolution of a coarse-grained spin-chain. Comparing with the experimental realizations performed with ultracold atoms in optical lattices [35], our results suggest that even if we are not able to fully resolve the system, entanglement can be still detected at some coarse-graining levels. With our approach, we showed that even if a detector cannot resolve the signal that comes from two or four neighboring qubits an entanglement wave can be still detected. Furthermore, we showed that it is possible to have some information about the microscopic entanglement even if we have access only to the coarse-graining description (3.23).

Therefore, our results evidence how the coarse-graining approach can play an important role in describing the detectability of quantum features in imprecise measurements scenarios. As already pointed out, such a topic is of fundamental importance in quantum technologies development, since nowadays experimentalists are able to control well-isolated quantum systems with an increasing number of qubits. Beyond that, as said in the introduction of this chapter, we hope that this approach represents a step toward elucidating the quantum-to-classical transition problem, bringing to the discussion more general mechanisms that perturb quantum resources beyond decoherence.

Chapter 4

Macro-to-micro quantum mapping and the emergence of nonlinearity

In this chapter, we will turn our attention to the opposite scenario studied in the last two chapters. Considering the universality of quantum mechanics, firstly, in Chapters 2 and 3, we formalized a coarse-graining channel as the general micro-to-macro mapping, and as an application we described the behavior of entanglement in macroscopic (effective) descriptions. Now, addressing the opposite direction, we will propose a macro-to-micro assignment that maps general macroscopic observations of a system to an ensemble of microscopic quantum states that the system could be in. As it will be presented, such an approach represents a step toward a general framework to understand the emergence of macroscopic behavior of nature. As an application, we will describe how effective stochastic nonlinear state dynamics emerge from linear deterministic microscopic evolutions. The content of this chapter is the subject of our recent preprint [49].

Traditionally, macro-to-micro assignments are the object of study of statistical physics [20]. From a general perspective, statistical mechanics, grounded on probability theory and statistical methods, explains macroscopic behavior of nature from the behaviors of large ensembles of microscopic constituents. In classical thermodynamics, for example, statistical mechanics successfully explains macroscopic properties, such as temperature, heat capacity, pressure, in terms of microscopic parameters. The open system scenario

is the usual paradigm of statistical mechanics. Considering the interaction between the system and environment, its main goal is to assign the proper microscopic ensemble to the macroscopic properties of a system – canonical and grandcanonical ensembles [20], for example.

Given the traditional framework presented above, aiming to shed some light towards a more general quantum statistical mechanics, we will propose a macro-to-micro mapping that overcomes the open quantum system scenario, showing that not only the locality of observables matter, but also how coarse-grained is our level of description.

Basically, such an approach is grounded on two basics premises:

1. Our perception of nature invariably arises through measurement processes. Whether considering the everyday perception of our surrounding environment or a sophisticated experimental setup, physical systems are fundamentally perceived and characterized in terms of measurement results of physical observables.

2. Our macroscopic perception of the world is inherently coarse-grained, with "classical" features emerging due to an effective description of quantum systems.

Following these premises, we formalize a macro-to-micro assignment, which we call averaging assignment map, that assigns to a set of macroscopic (coarse-grained) observations a microscopic description which is the ensemble-average of all compatible microscopic states. A pictorial representation of our approach is found in Figure 4.1.

In addition, as an application of our method, we use our averaging procedure as a framework to describe how macroscopic phenomena emerge from microscopic quantum mechanics. Specifically, we derive an effective state dynamical model which can be used to explain how nonlinear dynamics emerges from linear quantum mechanics, and we readily apply it to a state discrimination task.

This chapter is organized as follows: firstly, in Sec. 4.1 the macro-to-micro averaging assignment map will be formalized. As examples, we apply such a framework in the open quantum system, and in the blurred and saturated detection scenarios. In the sequence, in

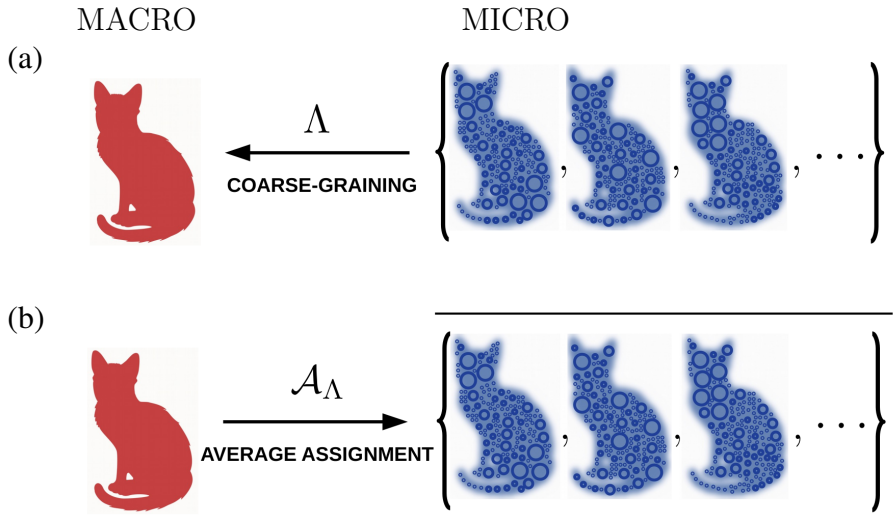

FIGURE 4.1: (a) **Micro-to-macro assignment.** In the right side, we pictorially represent in blue the set all microscopic states that are mapped through the coarse-graining operation Λ to a unique effective macroscopic state – represented by the red cat in the left. (b) **Macro-to-micro assignment**. The map $\mathcal{A}_\Lambda$ assigns to the system an ensemble given by the average over all microscopic states that comply with the macroscopic observations.

Sec. 4.2, by an operational procedure we derive an effective state dynamical approach. As an application, considering scenarios beyond the open quantum system scenario, we describe how nonlinear dynamics can emerge from microscopic linear quantum mechanics. As an application of this effective nonlinearity, in Sec. 4.3, we readily apply to the state dynamics in the blurred and saturated detection scenario in a discrimination task. Finally, in 4.4, we discuss the main conclusions and some perspectives.

4.1 The averaging assignment map

Let us start by defining the macro-to-micro assignment that was qualitatively described above. Such an approach is grounded on the coarse-graining maps formalized in Chapter 2, so it is convenient to start by doing a brief review. As discussed in Chapter 2, the coarse-graining channels play the role of general micro-to-macro mapping approach, which maps microscopic quantum states of a system to macroscopic (coarse-grained) states. As defined in (2.7), a coarse-graining map $\Lambda : \mathcal{L}(\mathcal{H}_D) \to \mathcal{L}(\mathcal{H}_d)$ is a CPTP map that connects

a microscopic level of description, with dimension D, to a macroscopic level with dimension d ($d < D$). Therefore, given a state $\psi \in \mathcal{L}(\mathcal{H}_D)$ describing a microscopic system, its related coarse-grained (macroscopic) description is $\Lambda[\psi] \in \mathcal{L}(\mathcal{H}_d)$.

After this brief review, we are now able to address the opposite direction. We want to define a procedure that maps a macroscopic (coarse-grained) description of a system, with d degrees of freedom, to a microscopic one, with D degrees of freedom (with $d < D$). Firstly, we assume that a macroscopic level of description is a coarse-grained version of a microscopic level, say by a coarse-graining map $\Lambda : \mathcal{L}(\mathcal{H}_D) \to \mathcal{L}(\mathcal{H}_d)$. Then, given a physical system described by a set $\mathcal{O} = \{o_i\}$ of $N_{\mathcal{O}}$ observed macroscopic quantities, quantum mechanics assigns to the underlying system a pure quantum state $\psi := |\psi\rangle\langle\psi| \in \mathcal{L}(\mathcal{H}_D)$ and observables $O_i \in \mathcal{L}(\mathcal{H}_d)$ such that $o_i = \mathrm{tr}[\Lambda[\psi]O_i]$.

In the scenario pictured above, note that the micro-state ψ satisfying the macroscopic constraints $\mathcal{O}$ is, however, not unique in general. We then define the set of all possible microscopic pure quantum states that abide by the macroscopic constraints:

$$\Omega_\Lambda(\mathcal{O}) = \big\{\psi \in \mathcal{L}(\mathcal{H}_D) \;\big|\; \mathrm{tr}[O_i\Lambda[\psi]\big] = o_i\,, \forall\, 1 \leq i \leq N_{\mathcal{O}}\big\}. \tag{4.1}$$

Therefore, in an operational perspective, when assembling an effective preparation with properties $\mathcal{O}$, which is accessed through a coarse-graining map Λ, microscopically we are in fact sampling from the set $\Omega_\Lambda(\mathcal{O})$. Due to the linearity of the expectation value, this perspective suggests an averaging assignment map $\mathcal{A}_\Lambda : \mathcal{O} \to \mathcal{L}(\mathcal{H}_D)$ that assigns the description to the microscopic ensemble:

$$\mathcal{A}_\Lambda[\mathcal{O}] \equiv \overline{\Omega_\Lambda(\mathcal{O})}^{\psi} = \int d\mu_\psi \mathrm{Pr}_\Lambda(\psi|\mathcal{O})\,\psi, \tag{4.2}$$

where $d\mu_\psi$ is the uniform Haar measure over pure states, and $\mathrm{Pr}_\Lambda(\psi|\mathcal{O})$ is the probability density of having the microscopic state ψ given the macroscopic constraints imposed by $\mathcal{O}$ and the coarse-graining map Λ. Note that $\mathrm{Pr}_\Lambda(\psi|\mathcal{O}) = 0$ for any $\psi \notin \Omega_\Lambda(\mathcal{O})$.

In the particular case where the set $\mathcal{O}$ is big enough as to allow for the full state reconstruction of ϱ in $\mathcal{L}(\mathcal{H}_d)$, i.e. $\mathcal{O}$ is tomographically complete, then $\mathcal{A}_\Lambda$ becomes a map between states, $\mathcal{A}_\Lambda : \mathcal{L}(\mathcal{H}_d) \to \mathcal{L}(\mathcal{H}_D)$:

$$\mathcal{A}_\Lambda[\varrho] = \overline{\Omega_\Lambda(\varrho)}^{\psi} = \int d\mu_\psi \mathrm{Pr}_\Lambda(\psi|\varrho)\, \psi, \tag{4.3}$$

with $\Omega_\Lambda(\varrho) = \{\psi \in \mathcal{L}(\mathcal{H}_D) \;\big|\; \Lambda[\psi] = \varrho\}$.

In general, the averaging assignment map – either in (4.2) or (4.3) –, is neither linear, with respect to the coarse-grained description, nor completely positive. Differently from the quantum operations defined in Section 2.1, these characteristics pose no fundamental problems or physical inconsistencies in the averaging assignment map. Briefly remembering, the quantum operation $\mathcal{E} : \mathcal{L}(\mathcal{H}_A) \to \mathcal{L}(\mathcal{H}_B)$, defined in (2.3), represents a general process that a physical system can undergo, with linearity and completely positivity being crucial properties that guarantee its physical consistency. Such properties are not fundamental in the averaging assignment map, since its physical meaning is quite different. The average procedure represents an inference about the microscopic state of the underlying coarse-grained observed system, not a physical process that the system undergoes. Therefore, the nonlinearity with respect to the macro observation poses no problem with superluminal communication [29], for example. Besides, since the action of the averaging map $\mathcal{A}_\Lambda$ gives a linear combination of the states in $\Omega_\Lambda(\varrho)$, it is clear that even when we extend the microscopic system by adding auxiliary systems, the average state will always produce a valid quantum state.

In the following, we will apply the averaging assignment map (4.3) in two distinct scenarios. Firstly, we will study how the open quantum system scenario fits in our averaging procedure, evaluating the average state considering the partial trace tr_E as the coarse-graining map. Next, our second example will be to calculate the averaging state related to the blurred and saturated detector map Λ_{BnS}.

4.1.1 Averaging assignment map: open quantum system

As discussed in 2.2.1, the partial trace plays a crucial role in the open quantum system scenario (system+environment). We assume that the effective description of the system is given by $\varrho_S \in \mathcal{L}(\mathcal{H}_S)$. No further constraints are assumed. In this case, the set of pure states of the system+environment is given by,

$$\Omega_{\mathrm{tr}_E}(\varrho_S) = \{\psi \in \mathcal{L}(\mathcal{H}_S \otimes \mathcal{H}_E) | \mathrm{tr}_E[\psi] = \varrho_S\}, \tag{4.4}$$

which is formed by the purifications of ϱ_S. As no further constraints are imposed, each purification appears with the same probability in $\Omega_{\mathrm{tr}_E}(\varrho_S)$. Thus, evaluating (4.3) in the partial trace case, we have:

$$\mathcal{A}_{\mathrm{tr}_E}[\varrho_S] = \varrho_S \otimes \frac{\mathbb{1}}{d_E}, \tag{4.5}$$

with $d_E = \dim(\mathcal{H}_E)$. The calculation of this result is shown in the Appendix A.1. Note that for the choice of partial trace as coarse-graining map, the averaging assignment map A_{tr_E} is linear in ϱ_S and completely positive.

Considering the open quantum system perspective, the above result have a reasonably straightforward meaning. Given that our effective level of knowledge allows us to consider only the description of the system, having complete ignorance about the environment and how it interacts with the system, the average map assign as the state of system+environment the product state between the reduced state of the system and the maximum mixture state of the environment.

4.1.2 Averaging assignment map: blurred and saturated detector

Now we turn our attention to the case of a blurred and saturated detection scenario analyzed in the Section 2.2.2, which is described by the coarse-graining map $\Lambda_{\mathrm{BnS}} : \mathcal{L}(\mathcal{H}_4) \to \mathcal{L}(\mathcal{H}_2)$ defined in (2.10).

Then, to a preparation of a system given by an effective qubit $\varrho \in \mathcal{L}(\mathcal{H}_2)$, quantum mechanics assigns to the underlying system a pure quantum state $\psi \in \mathcal{L}(\mathcal{H}_4)$ such that $\varrho = \Lambda_{\mathrm{BnS}}[\psi]$. So, as stated by the average procedure, the description at the microscopic level is given by $\mathcal{A}_{\Lambda_{\mathrm{BnS}}}[\varrho]$, meaning that we need to take the average over the states belonging to the set

$$\Omega_{\Lambda_{\mathrm{BnS}}}(\varrho) = \{\psi \in \mathcal{L}(\mathcal{H}_4) | \Lambda_{\mathrm{BnS}}[\psi] = \varrho\}. \tag{4.6}$$

In order to better present the results, we write the elements of ϱ in the computational basis as

$$\varrho = \begin{pmatrix} \varrho_{00} & \varrho_{01} \\ \varrho_{01}^* & \varrho_{11}. \end{pmatrix}, \tag{4.7}$$

Then calculating (4.3), the averaging assignment procedure gives:

$$\mathcal{A}_{\Lambda_{\mathrm{BnS}}}[\varrho] = \begin{pmatrix} \varrho_{00} & \frac{\varrho_{01}}{\sqrt{3}} & \frac{\varrho_{01}}{\sqrt{3}} & \frac{\varrho_{01}}{\sqrt{3}} \\ \frac{\varrho_{01}^*}{\sqrt{3}} & \frac{\varrho_{11}}{3} & \frac{|\varrho_{01}|^2}{2\varrho_{00}} - \frac{\varrho_{11}}{6} & \frac{|\varrho_{01}|^2}{2\varrho_{00}} - \frac{\varrho_{11}}{6} \\ \frac{\varrho_{01}^*}{\sqrt{3}} & \frac{|\varrho_{01}|^2}{2\varrho_{00}} - \frac{\varrho_{11}}{6} & \frac{\varrho_{11}}{3} & \frac{|\varrho_{01}|^2}{2\varrho_{00}} - \frac{\varrho_{11}}{6} \\ \frac{\varrho_{01}^*}{\sqrt{3}} & \frac{|\varrho_{01}|^2}{2\varrho_{00}} - \frac{\varrho_{11}}{6} & \frac{|\varrho_{01}|^2}{2\varrho_{00}} - \frac{\varrho_{11}}{6} & \frac{\varrho_{11}}{3} \end{pmatrix}. \tag{4.8}$$

The calculation is detailed in the Appendix A.2.

Observe that differently from the average state related to the partial trace case (4.5), for the blurred and saturated detector the assigned average state is nonlinear on ϱ. Note that the nonlinear terms are related to the coherences within the excited subspace span($\{|01\rangle$, $|10\rangle$,$|11\rangle\}$), which are exactly the states that the blurry detector cannot resolve. Thus, all these nonlinear terms vanish after the blurred and saturated coarse-graining map is applied. However, as it will be shown in the next section, in the effective state dynamics, this nonlinearity can appear, allowing for the emergence of nonlinear processes.

4.2 Effective state dynamics

Now that we know how to connect macroscopic to microscopic descriptions through the averaging assignment map, we will establish an operational procedure that characterizes how general stochastic effective dynamics arise from deterministic unitary quantum dynamics.

In order to construct the effective (macroscopic) description of a dynamical process of a system, our approach will assume access only to the coarse-graining map that describes our ability to construe the microscopic world, and to a model of the underlying quantum microscopic dynamics.

More explicitly, given an initial effective state $\varrho(0) \in \mathcal{L}(\mathcal{H}_d)$, we want to construct a family of effective dynamical maps $\Gamma_t : \mathcal{L}(\mathcal{H}_d) \to \mathcal{L}(\mathcal{H}_d)$, such that for each time $t \in \mathbb{R}_+$ the evolved effective state is given by

$$\varrho(t) = \Gamma_t[\varrho(0)], \tag{4.9}$$

Once again we appeal to the operational mindset in order to obtain Γ_t. Our procedure is inspired in the quantum state tomography (QST) task, which requires a sufficiently large set of initial identical preparations of the system in order to completely reconstruct its quantum state. One way of thinking is, to prepare the initial effective state $\varrho(0) \in \mathcal{L}(\mathcal{H}_d)$ means, in each run, to prepare a microscopic state from the set

$$\Omega_\Lambda(\varrho(0)) = \{\psi \in \mathcal{L}(\mathcal{H}_D) | \Lambda[\psi] = \varrho(0)\}. \tag{4.10}$$

Let $\psi^{(i)}(0) \in \Omega_\Lambda(\varrho(0))$ be the microstate selected, with probability $\mathrm{Pr}_\Lambda(\psi^{(i)}(0)|\varrho(0))$, in the i-th run. Microscopically, this state evolves through the unitary map $\mathcal{U}_t$, and then to obtain its effective description we apply the coarse-graining map Λ. All this leads, in the i-th run, to $\varrho^{(i)}(t) = (\Lambda \circ \mathcal{U}_t)[\psi^{(i)}(0)]$ – see Figure 4.2 (a). If we are to determine the final effective state, for instance via quantum state tomography (QST), this procedure has to be

performed many times, and an averaging naturally appears:

$$\begin{aligned}\varrho(t) &= \int d\mu_{\psi(0)} \mathrm{Pr}_\Lambda(\psi(0)|\varrho(0))\ (\Lambda \circ \mathcal{U}_t)[\psi(0)] \\ &= (\Lambda \circ \mathcal{U}_t) \left[\int d\mu_{\psi(0)} \mathrm{Pr}_\Lambda(\psi(0)|\varrho(0))\psi(0) \right]. \end{aligned} \tag{4.11}$$

In the second line above we used the linearity of both the unitary evolution and coarse-graining channel. Note that the integral in (4.11) is the very definition of the averaging assignment map acting on $\varrho(0)$. Combining all the three steps, the effective dynamical map $\Gamma_t : \mathcal{L}(\mathcal{H}_d) \to \mathcal{L}(\mathcal{H}_d)$ is obtained as:

$$\Gamma_t = (\Lambda \circ \mathcal{U}_t \circ \mathcal{A}_\Lambda), \tag{4.12}$$

with (4.9) rewritten as

$$\begin{aligned}\varrho_t &= \Gamma_t[\varrho(0)] \\ &= (\Lambda \circ \mathcal{U}_t \circ \mathcal{A}_\Lambda)[\varrho(0)]. \end{aligned} \tag{4.13}$$

The construction of the effective coarse-grained dynamical model is schematically represented in Fig. 4.2 (b).

The evolved state (4.13), in general, will be nonlinear as a function of the initial effective state $\varrho(0)$, and not completely positive. These properties come from the averaging assignment map (4.3), which, is nonlinear and not completely positive. However, as discussed in the last chapter, such properties pose no physical problems, since $\mathcal{A}_\Lambda$ is not a physical process that the system undergoes, but an inference about its microscopic quantum description, given our coarse-grained information. Note that the effective dynamical map $\Gamma_t = (\Lambda \circ \mathcal{U}_t \circ \mathcal{A}_\Lambda)$, is defined as a composition of three maps, where $\mathcal{U}_t$ and Λ represent physical processes which the system undergoes, and both are linear

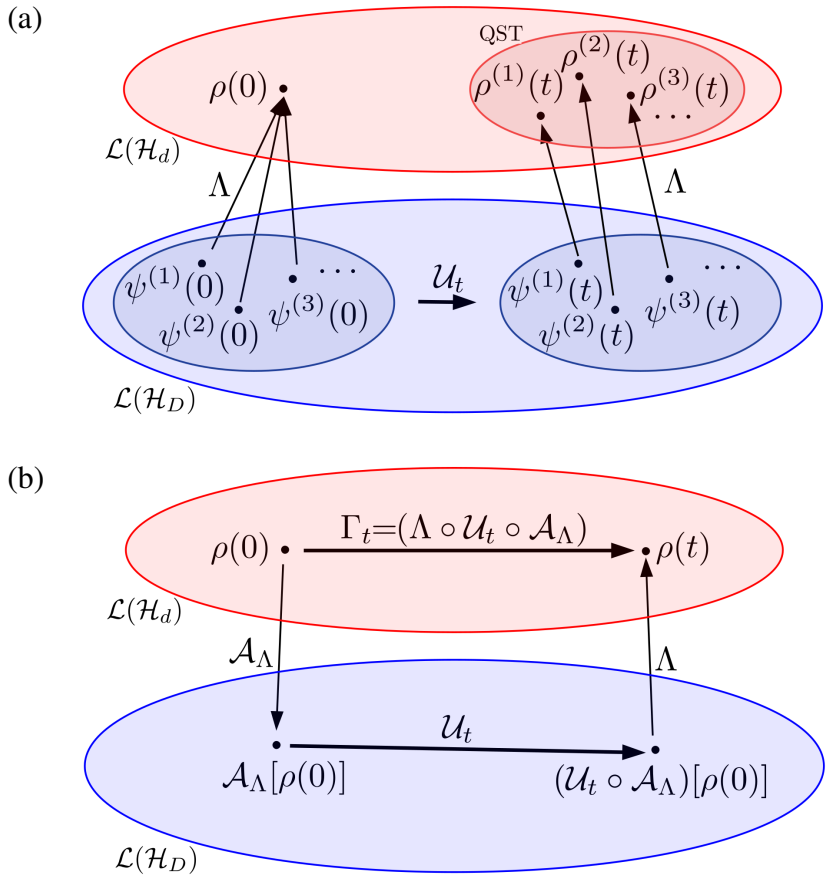

FIGURE 4.2: (a) **Single run evolution.** In the i-th run, the preparation of $\varrho(0)$ implies the random preparation of a microscopic state $\psi^{(i)}(0) \in \Omega_\Lambda(\varrho(0))$, which then evolves according to the unitary map $\mathcal{U}_t$, and through the coarse-graining map Λ finally gives the effective state $\varrho^{(i)}(t) = (\Lambda \circ \mathcal{U}_t)[\psi^{(i)}(0)]$. In each run a possibly different effective state is created. (b) **Effective evolution.** The scheme in (a), together with the linearity of quantum mechanics, suggests an effective dynamics given by $\Gamma_t = (\Lambda \circ \mathcal{U}_t \circ \mathcal{A}_\Lambda)$.

and CPTP. Therefore, by construction, the nonlinearity manifested in (4.13) is an effective phenomenon observed in macroscopic levels of description. Thus (4.13) does not represent any disagreement with microscopic linear quantum mechanics, superluminal communication remains forbidden [29].

4.2.1 Effective state dynamics: open quantum system

In the partial trace case, the description of the whole system and environment fulfilling the constraint is given by the averaging assignment map, $\mathcal{A}_{\mathrm{tr}_E}[\varrho(0)] = \varrho(0) \otimes \frac{\mathbb{1}}{d_E}$. From

(4.12), in this open quantum system scenario, the effective evolved state ϱ_t is obtained as follows:

$$\varrho(t) = (\mathrm{tr}_E \circ \mathcal{U}_t)[\varrho(0) \otimes \frac{\mathbb{1}}{d_E}]. \tag{4.14}$$

Note that the effective dynamics in this case is linear on $\varrho(0)$, since both the unitary evolution $\mathcal{U}_t$ and the coarse-graining map tr_E are linear operations. Moreover, as $\mathcal{U}_t$ and tr_E are completely positive, so is Γ_t.

From (4.14) we can analyze a simple scenario of a local unitary evolution. With $\mathcal{U}_t = \mathcal{U}_t^S \otimes \mathcal{U}_t^E$, the unitary evolution:

$$\begin{aligned}\varrho(t) =& (\mathrm{tr}_E \circ \mathcal{U}_t^S \otimes \mathcal{U}_t^E)[\varrho(0) \otimes \frac{\mathbb{1}}{d_E}] \\ =& \mathcal{U}_t^S[\varrho(0)]\end{aligned} \tag{4.15}$$

is recovered, so the effective evolution $\Gamma_t = \mathcal{U}_t^S$, more than linear, it is unitary.

4.2.2 Effective state dynamics: blurred and saturated detector

As previously discussed, the average state in the detector case, Eq.(4.8), has a nonlinear dependence on the coarse-grained state. This may lead to a nonlinear effective dynamics if we allow the composite system to evolve before the application of the coarse-graining map. For the nonlinearity in the average state to imply a nonlinear effective dynamics, an appropriate unitary evolution must be chosen so that the nonlinear term in (4.8) shows up in elements other than the single excitation subspace coherences, as those vanish by the action of Λ_{BnS}.

As an example, we start by considering the initial coarse-grained state $\varrho(0) \in \mathcal{L}(\mathcal{H}_2)$:

$$\varrho(0) = \begin{pmatrix} \frac{1}{2} & \varrho_{01}(0) \\ \varrho_{01}(0) & \frac{1}{2} \end{pmatrix}, \tag{4.16}$$

with $\varrho_{01}(0) \in \mathbb{R}_+$, to simplify the analysis.

Given that $\varrho(t) = (\Lambda_{\mathrm{BnS}} \circ \mathcal{U}_t \circ \mathcal{A}_{\Lambda_{\mathrm{BnS}}})[\varrho(0)]$, the first step is the average state $\mathcal{A}_{\Lambda_{\mathrm{BnS}}}[\varrho(0)]$, which can be easily constructed following the general form given by the equation (4.8).

The next step is the microscopic evolution. We consider the unitary evolution generated by the local Hamiltonian $H = \hbar\omega \mathbb{1} \otimes \sigma_y$, i.e., the unitary evolution of the averaged assigned state is given by $\mathcal{U}_t[\mathcal{A}_{\Lambda_{\mathrm{BnS}}}[\varrho(0)]] = U_t \mathcal{A}_{\Lambda_{\mathrm{BnS}}}[\varrho(0)] U_t^\dagger$ with $U_t = \exp[-\mathrm{i}\omega t(\mathbb{1} \otimes \sigma_y)]$.

Finally, we apply the coarse-graining map Λ_{BnS}, given by (2.10). Under these circumstances, the evolved coarse-grained effective description at $\omega t = \pi/3$ is given by:

$$\varrho(\pi/3\omega) = \frac{1}{16}\begin{pmatrix} (1-2\varrho_{01}(0))^2 & \dfrac{(1-2\varrho_{01}(0))^2(1+2\varrho_{01}(0))}{2} \\ \dfrac{(1-2\varrho_{01}(0))^2(1+2\varrho_{01}(0))}{2} & 1-(1-2\varrho_{01}(0))^2 \end{pmatrix} \tag{4.17}$$

Clearly, it shows a nonlinear dependence on the initial state.

As it will be explored in the following, such a nonlinear character can be used in a state discrimination task, then gaining added value in effective quantum information processing protocols.

4.3 Applications: Effective state discrimination

Nonlinear dynamical models have far-reaching applications, ranging from condensed matter physics to the description of biological systems [50]. In the following, we show that the nonlinear dynamics shown above can be useful in the task of discriminating between two effective states.

4.3.1 State discrimination

In essence, quantum state discrimination describes the distinguishability of different quantum states, and the general process of extracting classical information from quantum systems [51]. Such a state discrimination task underlies various applications in quantum

information processing, as an example, in the characterization of mutual information in cryptography protocols [52, 53].

Since our goal is to give an example of a useful application of the effective nonlinear dynamics, it will be sufficient to present only a simplified discrimination scheme.

Consider a quantum communication channel composed of two parts: the sender (S), who controls a source, and the receiver (R), who controls a measurement device. The source can generate two states: ϱ or χ in $\mathcal{L}(\mathcal{H})$. It is known to both parties – S and R – that, in each run, S sends to R one of these two states (either ϱ or χ) with probability $1/2$. So just before the measurement, from R's perspective, the system is described by a probabilistic mixture: $\varrho/2 + \chi/2$. Then, R performs the measurement. Finally, in such a single-shot communication procedure, R can learn about the state sent by S from the detection outcome produced by the measurement. This is the quantum state discrimination scheme, and it is represented in Figure 4.3.

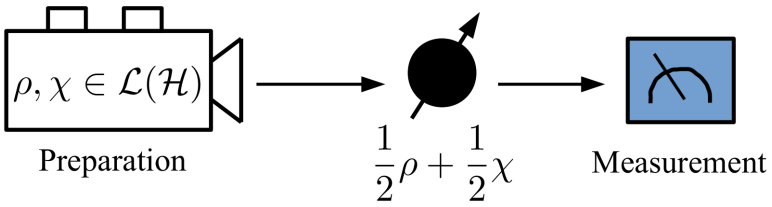

FIGURE 4.3: **Quantum state discrimination scheme.**

In this scenario, the so-called Helstrom bound [54], one foundational result in quantum information theory, tells that the maximum probability of a single-shot measurement to correctly identify which state was produced by the source device, is given by

$$\left(1 + \mathcal{D}(\varrho, \chi)\right)/2, \tag{4.18}$$

where $\mathcal{D}(\varrho, \chi) = \mathrm{tr}|\varrho - \chi|/2$ is the trace distance between the states. Therefore, the larger the distance between the two states, the bigger is the probability of distinguishing between them.

Another central result of quantum information theory is that the distance between two states does not increase by the action of a linear CPTP map $\mathcal{E} : \mathcal{L}(\mathcal{H}_A) \to \mathcal{L}(\mathcal{H}_B)$, i.e.,

$$\mathcal{D}(\mathcal{E}[\varrho], \mathcal{E}[\chi]) \leq \mathcal{D}(\varrho, \chi). \tag{4.19}$$

As such, the probability of distinguishing between two states cannot increase by further linear processing of the system.

4.3.2 Effective state discrimination

Now assume that the receiver (R) wants to distinguish between two effective states, and he had access to a nonlinear dynamics given by an effective dynamical channel of the form (4.12). In this case the probability of discriminating between two states can in fact increase, as it will be shown.

For concreteness, assume the discrimination scenario described above, with a source being able to generate the coarse-grained states $\varrho(0) = \mathbb{1}/2$ or $\chi(0) = |\chi\rangle\langle\chi|$ (with $|\chi\rangle = \sqrt{0.8}|0\rangle + \sqrt{0.2}|1\rangle$). Now, before the measurement, R is able to apply the effective dynamical channel $\Gamma_t = (\Lambda \circ \mathcal{U}_t \circ \mathcal{A}_\Lambda)$. Let the coarse-graining channel be the Λ_{BnS}, and the microscopic dynamics be governed by the Hamiltonian $H = \hbar\omega(\mathbb{1} \otimes \sigma_y + \sigma_y \otimes \mathbb{1})$ – See Figure 4.4 (a). In this case, the effective channel Γ_t is nonlinear, and as shown in Fig. 4.4 (b) the distance among the two effective states can be bigger than its initial value, allowing therefore for a better effective state discrimination.

It must be stressed that the increase in state discrimination is only possible in the effective level. Since $\Gamma_t = (\Lambda \circ \mathcal{U}_t \circ \mathcal{A}_\Lambda)$, defining $\varrho' = \mathcal{A}_\Lambda[\varrho(0)]$, $\chi' = \mathcal{A}_\Lambda[\chi(0)]$ and $\mathcal{E}' = (\Lambda \circ \mathcal{U}_t)$, in (4.19), it is simple to see that:

$$\mathcal{D}(\Gamma_t[\varrho(0)], \Gamma_t[\chi(0)]) \leq \mathcal{D}(\mathcal{A}_{\Lambda_{\text{BnS}}}[\varrho(0)], \mathcal{A}_{\Lambda_{\text{BnS}}}[\chi(0)]). \tag{4.20}$$

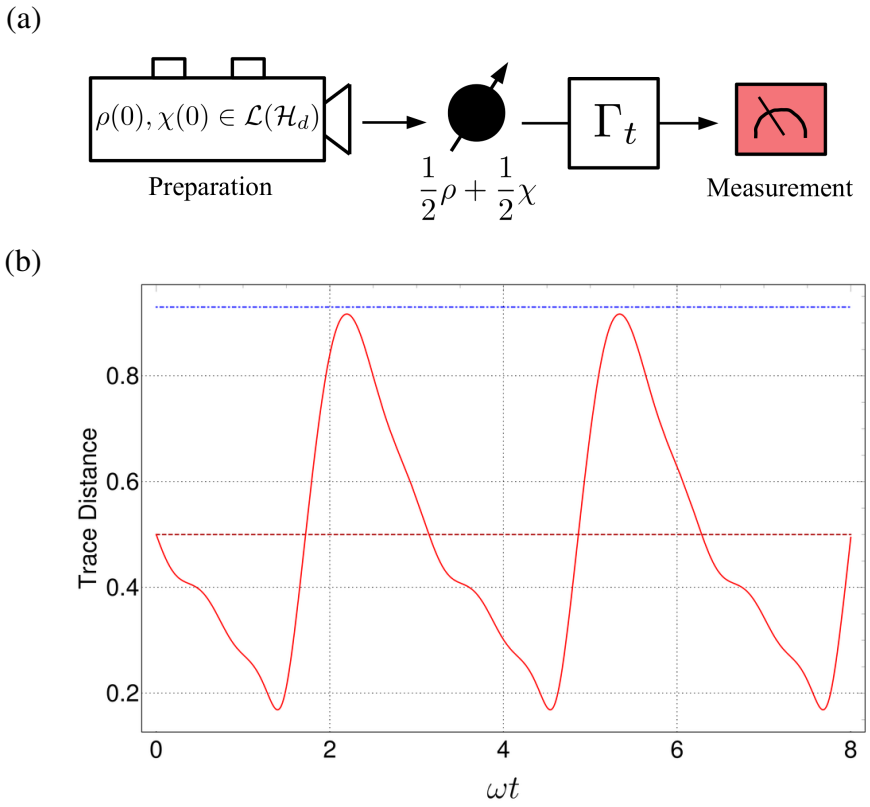

FIGURE 4.4: **Effective distance evolution.** (a) Coarse-grained quantum discrimination scheme (b) The distance between two effective system's description can increase due to a nonlinear coarse-grained dynamics. The red solid line describes the distance evolution $\mathcal{D}(\varrho(t), \chi(t))$; the red dashed line represents the initial distance $\mathcal{D}(\varrho(0), \chi(0))$; while the blue dot-dashed line shows the distance between the underlying assignments $\mathcal{D}(\mathcal{A}_{\Lambda_{\text{BnS}}}[\varrho(0)], \mathcal{A}_{\Lambda_{\text{BnS}}}[\chi(0)])$.

Thus the best effective discrimination is never better than the best microscopic discrimination. If it were possible to increase the success of discriminating between two states by throwing away some information, besides astonishing, it would also violate the non-signaling principle [29, 55].

4.4 Summary and conclusions

In this chapter, employing quantum information tools, we formalized a general macro-to-micro assignment. Going beyond the open quantum system paradigm, not only the locality of observables matter, but also how coarse-grained is our level of description. In

this sense, we are convinced that our approach offers a contribution towards a generalized quantum statistical mechanics, enlarging the usual scenario where we have a clear split between system and environment, to an extended definition of subsystems.

From this approach, looking at the stochastic effective state dynamics, nonlinear evolutions may emerge naturally from the deterministic unitary linear quantum dynamics. Again the level of description, and thus the ability to prepare and describe macroscopic systems, is the key. Through our averaging procedure, it became clear that fixing a coarse-grained preparation is usually not sufficient to determine the underlying quantum pure state. As we exemplify in the blurred and saturated scenario, the best suited description of the microscopic state is possibly nonlinear on the macroscopic description. This effective nonlinearity can be, in general, expressed in the dynamical process, but introduces no conflict with the physical tenets of complete positivity and no-signaling.

The present framework may have impact not only on foundational aspects – like the quantum-to-classical transition –, but also in more applied topics – such as in quantum communication protocols that exploit the discrimination between effective states.

Chapter 5

Conclusions and Perspectives

In this last chapter, we summarize and discuss the leading results of this thesis. We also list perspectives for the continuity of our work, mentioning the developments such contributions may take.

Universality of quantum mechanics

As discussed in Chapter 1, if we assume quantum mechanics as a fundamental theory of physics, quantum mechanics inherits a universal status. It means that, at least in principle, the theory must assign a quantum state to any level of description of a system. The universality of quantum mechanics implies a two-way describing nature. In the first one, a *micro-to-macro* mapping, the theory must describe how to connect microscopic quantum states of a system to macroscopic/effective descriptions of a physical system. In the second and opposite direction, a *macro-to-micro* mapping, quantum mechanics assigns to a macroscopic description an ensemble of microscopic quantum states that the system could be in.

Micro-to-macro mapping

To deal with the micro-to-macro mapping, in Chapter 2, we formalized a general coarse-graining operation that maps microscopic quantum states to macroscopic states. The

coarse-graining map was defined as a quantum operation (a linear and CPTP map) that lowers the dimension of the microscopic state of a system. We showed that the coarse-graining formalism generalizes the open quantum system paradigm, since it models scenarios where rather than the locality of observables, the blurriness of the level of description is the determinant feature. In this sense, we are convinced that the coarse-graining approach offers a more general framework to study macroscopic/effective descriptions of a physical system that may emerge from microscopic quantum mechanics.

As an illustration, still in Chapter 2, we have presented two coarse-graining situations. The first one was the usual open quantum system scenario, where the description of the system of interest is described by tracing out the degrees of freedom of its environment. In this case, given a clear split between the system and environment, the partial trace tr_E plays the role of coarse-graining map, getting rid of the environment's degrees of freedom. The second physical situation was an imperfect detection of a spin-system in an optical lattice. Inspired by the fluorescence imaging technique [32], we constructed a coarse-graining map Λ_{BnS} that models a blurred and saturated spin-detection, and, as demonstrated, such a coarse-graining situation does not fit in the open quantum system scenario.

In sequence, in Chapter 3, we explored the blurred and saturated coarse-graining map Λ_{BnS} as a tool to describe spin-entanglement in an optical lattice scenario considering a range of coarse-grained resolution. Comparing it with recent experimental realizations performed with ultracold atoms [35], it allows us to conjecture up to what limit the lack of resolution of the equipment compromises the detection of quantum entanglement. Such application demonstrates how the coarse-graining formalism can be a promising framework to investigate the fragility of genuine quantum features to different levels of imprecise (and less costly) measuring processes. In addition, the coarse-graining approach sheds some light on the characterization of the quantum-to-classical transition. Different from the traditional decoherence theory, which is placed on the open quantum system paradigm, the coarse-graining approach brings to the discussion other mechanisms that

disturb quantum resources without necessarily resorting to the interaction between system and environment.

Once summarized our main results concerning the *micro-to-macro* mapping, we list two main perspectives about possible improvements in our model and further applications:

- Apply our coarse-graining model to other physical scenarios, modeling other coarse-grained situations and describing the behavior of different quantum features.
- A generalization in the definition of coarse-grained maps by considering non-completely positive maps.

The first point concerns the extension of the application of the blurred and saturated coarse-graining map to other physical circumstances. Nowadays, ultracold atoms in an optical lattice represent a prominent platform for the simulation of a range of other quantum many-body problems [37, 33]. Part of this success is due to the development of high-precision detection devices such as quantum gas microscopes [32, 37]. Since our coarse-graining is constructed to model this kind of detection, we hope that our model will be relevant for other ultracold-atom-based quantum simulations. Viable possibilities are to probe quantum magnetism, to realize and detect topological matter, and to study quantum systems with long-range interactions [37, 33]. Situations where more than one excitation is present in the system, and the full XXZ Hamiltonian (such as in Refs. [58, 59]), can also be directly modeled by our map. Moreover, given its simplicity and intuitive construction, we expect that this coarse-graining approach will be adapted and extended to other experimental achievements in which detection cannot be made with proper accuracy.

The second point is motivated by the results of two works, [56] and [57]. The authors argued that complete positivity (CP) is not a requirement for a good representation of general quantum transformation. Their calculations suggest that to get a full understanding of quantum transformations, non-completely positive maps should be considered as well. Our coarse-graining map is formalized inspired by the quantum operation definition

which requires complete positivity, so if we dismiss the CP constraint, we can, at first sight, define a more general coarse-graining map. This is a step that must be taken with caution, an in-depth study is needed to verify the physical consistency.

Macro-to-micro mapping

In Chapter 4, we formalized a macro-to-micro model: the averaging assignment map $\mathcal{A}_\Lambda$. Considering a set of coarse-grained observations that macroscopically characterizes a system, the averaging map $\mathcal{A}_\Lambda$ assigns to this macroscopic description a microscopic average-ensemble of all pure quantum states that obey the observed data. Grounded on the coarse-graining formalism, the averaging assignment goes beyond the open quantum system scenario. Our results demonstrate that a more general macro-to-micro assignment needs to account not only for the locality of the observations but also to describe how coarse-grained is the level of description. Therefore, by extending the definition of subsystem to scenarios that do not present a clear split between system and environment, we are convinced that the average assignment approach represents a contribution towards generalized statistical mechanics.

If in fact, the average assignment procedure represents the mechanism that properly connects macroscopic descriptions with microscopic quantum mechanics; such an approach must play an important role in elucidating emergent phenomena in physics [21] from first principles. That is, the averaging assignment map must be a tool to describe how emerging macroscopic behavior is in accordance with the underlying quantum mechanics rules. To illustrate such an idea, as a by-product of our averaging assignment approach, we defined an effective state dynamic map that naturally emerges from deterministic linear quantum mechanics. As a consequence of the nonlinearity of $\mathcal{A}_\Lambda$ in the blurred and saturated, we showed how effective nonlinear dynamics naturally emerges from linear quantum evolution. As a application, we employed such nonlinear dynamic in a state discrimination task.

Proceeding in the same way as in the previous section, we now list some ideas about possible improvements in our macro-to-micro assignment and further applications:

- Study how different the averaging assignment is from the usual maximum entropy method.

- Explore the nonlinearity of our effective state dynamical map to investigate how chaotic dynamics can emerge from microscopic quantum mechanics.

Let us clarify each point above. The first point is to describe an alternative macro-to-micro assignment inspired by a more traditional approach. Remember that the averaging assignment map connects a coarse-grained description to an ensemble that is the average of the set of pure states that abide by the coarse-graining constraint. However, alternatively we could construct the ensemble that maximizes the entropy. Such approach is inspired by quantum statistical mechanics, which says that the state that better describes a system defined by a Hamiltonian H, in thermal equilibrium with a heat bath at temperature T is given by the Gibbs state:

$$\chi^{\mathrm{G}} = \frac{1}{Z}\exp[-\beta H] \tag{5.1}$$

with β is such that satisfies $\mathrm{tr}(H\chi^{\mathrm{G}}) = E$ and $Z = \mathrm{tr}[\exp(-\beta H)]$ is called the partition function. This state maximizes the von Neumann entropy, $S(\psi) = -\mathrm{tr}\,\psi\ln\psi$, of the state subjected to the fixed average energy constraint [19, 20]. Transporting this scheme to a coarse-graining description, at first, the idea would be instead of an fixed energy constraint, we define our assigned microscopic state as the maximum entropic mixture related to the set $\Omega(\varrho) = \{\psi \in \mathcal{L}(\mathcal{H}_D)|\Lambda[\psi] = \varrho\}$.

Characterizing the macro-to-micro assignment using the maximum entropic principle may lead to relevant differences in macroscopic predictions if compared with the averaging method. Such difference must become evident if we look at the effective state

dynamics $\Gamma_t = \Lambda \circ \mathcal{U}_t \circ \mathcal{A}_\Lambda$, for example. Note that if we replace the averaging assignment $\mathcal{A}_\Lambda$ by the maximum entropy procedure, the effective dynamics Γ_t fundamentally changes. Therefore, we think that the disagreement between averaging and maximum entropy procedures would be a key issue to properly describe macroscopic phenomena.

The second point is motivated by the crucial role of nonlinear dynamics in the manifestation of chaotic behavior [60]. Different from models where nonlinear dynamics are obtained via specific phenomenological approximations [60, 61], our nonlinear effective state dynamic model could be a route for elucidating the emergence of chaotic behavior from first principles. Even though presented in this vague way, we think it is important to mention this possible application of our approach.

Finally, we conclude this thesis, leaving open a possible experimental verification of our macro-to-micro model. Since the construction of the averaging assignment map and, consequently, the effective state dynamics model are easily related to an operational scenario of quantum state tomography, our procedure becomes, at least in principle, favorably open for experimental testing.

Bibliography

[1] B. Povh, K. Rith, and F. Zetsche, *Particles and nuclei*, vol. 4. Springer, 1995.

[2] B. Odom, D. Hanneke, B. d'Urso, and G. Gabrielse, "New measurement of the electron magnetic moment using a one-electron quantum cyclotron," *Physical Review Letters*, vol. 97, no. 3, p. 030801, 2006.

[3] M. D. Schwartz, *Quantum field theory and the standard model*. Cambridge University Press, 2014.

[4] D. Stamper-Kurn, M. Andrews, A. Chikkatur, S. Inouye, H.-J. Miesner, J. Stenger, and W. Ketterle, "Optical confinement of a bose-einstein condensate," *Physical Review Letters*, vol. 80, no. 10, p. 2027, 1998.

[5] R. Horodecki, P. Horodecki, M. Horodecki, and K. Horodecki, "Quantum entanglement," *Reviews of Modern Physics*, vol. 81, no. 2, p. 865, 2009.

[6] C.-K. Chan, *Theory and application of open quantum systems*. PhD thesis, UC San Diego, 2012.

[7] F. Arute, K. Arya, R. Babbush, D. Bacon, J. C. Bardin, R. Barends, R. Biswas, S. Boixo, F. G. Brandao, D. A. Buell, *et al.*, "Quantum supremacy using a programmable superconducting processor," *Nature*, vol. 574, no. 7779, pp. 505–510, 2019.

[8] V. Havlíček, A. D. Córcoles, K. Temme, A. W. Harrow, A. Kandala, J. M. Chow, and J. M. Gambetta, "Supervised learning with quantum-enhanced feature spaces," *Nature*, vol. 567, no. 7747, pp. 209–212, 2019.

[9] M. W. Johnson, M. H. Amin, S. Gildert, T. Lanting, F. Hamze, N. Dickson, R. Harris, A. J. Berkley, J. Johansson, P. Bunyk, *et al.*, "Quantum annealing with manufactured spins," *Nature*, vol. 473, no. 7346, p. 194, 2011.

[10] H. Häffner, W. Hänsel, C. Roos, J. Benhelm, M. Chwalla, T. Körber, U. Rapol, M. Riebe, P. Schmidt, C. Becher, *et al.*, "Scalable multiparticle entanglement of trapped ions," *Nature*, vol. 438, no. 7068, pp. 643–646, 2005.

[11] M. A. Nielsen and I. L. Chuang, *Quantum Computation and Quantum Information*. Cambridge University Press, 2000.

[12] J. Kempe, "Multiparticle entanglement and its applications to cryptography," *Physical Review A*, vol. 60, no. 2, p. 910, 1999.

[13] T. Jennewein, C. Simon, G. Weihs, H. Weinfurter, and A. Zeilinger, "Quantum cryptography with entangled photons," *Physical Review Letters*, vol. 84, no. 20, p. 4729, 2000.

[14] R. Alicki, M. Fannes, and M. Pogorzelska, "Quantum generalized subsystems," *Phys. Rev. A*, vol. 79, p. 052111, May 2009.

[15] C. Duarte, G. D. Carvalho, N. K. Bernardes, and F. de Melo, "Emerging dynamics arising from coarse-grained quantum systems," *Phys. Rev. A*, vol. 96, p. 032113, Sep 2017.

[16] P. Silva Correia and F. de Melo, "Spin-entanglement wave in a coarse-grained optical lattice," *Phys. Rev. A*, vol. 100, p. 022334, Aug 2019.

[17] O. Kabernik, J. Pollack, and A. Singh, "Quantum state reduction: Generalized bipartitions from algebras of observables," *Phys. Rev. A*, vol. 101, p. 032303, Mar 2020.

[18] C. Duarte, G. D. Carvalho, N. K. Bernardes, and F. de Melo, "Emerging dynamics arising from coarse-grained quantum systems," *Physical Review A*, vol. 96, no. 3, p. 032113, 2017.

[19] K. Huang, *Introduction to statistical physics*. Chapman and Hall/CRC, 2009.

[20] R. Balian, *From Microphysics to Macrophysics: Methods and Applications of Statistical Physics*. Springer Science & Business Media, 2007.

[21] J. L. Lebowitz, "Emergent phenomena," *Physik Journal*, vol. 6, no. 8/9, p. 41, 2007.

[22] S. Kmiecik, D. Gront, M. Kolinski, L. Wieteska, A. E. Dawid, and A. Kolinski, "Coarse-grained protein models and their applications," *Chemical reviews*, vol. 116, no. 14, pp. 7898–7936, 2016.

[23] M. G. Saunders and G. A. Voth, "Coarse-graining methods for computational biology," *Annual review of biophysics*, vol. 42, pp. 73–93, 2013.

[24] K. Hwang and N. Jotwani, *Advanced Computer Architecture, 3e*. McGraw-Hill Education, 2016.

[25] P. Ehrenfest and T. Ehrenfest, *The conceptual foundations of the statistical approach in mechanics*. Courier Corporation, 1990.

[26] L. P. Kadanoff, "Scaling laws for ising models near T_c," *Physics Physique Fizika*, vol. 2, pp. 263–272, Jun 1966.

[27] K. G. Wilson, "The renormalization group: Critical phenomena and the kondo problem," *Rev. Mod. Phys.*, vol. 47, pp. 773–840, Oct 1975.

[28] N. Goldenfeld, *Lectures on phase transitions and the renormalization group*. CRC Press, 2018.

[29] N. Gisin, "Weinberg's non-linear quantum mechanics and supraluminal communications," *Phys. Lett. A*, vol. 143, no. 1-2, pp. 1–2, 1990.

[30] L. Aolita, F. de Melo, and L. Davidovich, "Open-system dynamics of entanglement: a key issues review," *Reports on Progress in Physics*, vol. 78, no. 4, p. 042001, 2015.

[31] P. S. Correia, "Entanglement in Coarse-grained Systems," Master's thesis, Centro Brasileiro de Pesquisas Físicas, Rio de Janeiro - RJ, 2017.

[32] J. F. Sherson, C. Weitenberg, M. Endres, M. Cheneau, I. Bloch, and S. Kuhr, "Single-atom-resolved fluorescence imaging of an atomic mott insulator," *Nature*, vol. 467, no. 7311, pp. 68–72, 2010.

[33] H. Ott, "Single atom detection in ultracold quantum gases: a review of current progress," *Reports on Progress in Physics*, vol. 79, p. 054401, apr 2016.

[34] R. Blatt and C. F. Roos, "Quantum simulations with trapped ions," *Nature Physics*, vol. 8, no. 4, pp. 277–284, 2012.

[35] T. Fukuhara, S. Hild, J. Zeiher, P. Schauß, I. Bloch, M. Endres, and C. Gross, "Spatially resolved detection of a spin-entanglement wave in a bose-hubbard chain," *Physical Review Letters*, vol. 115, no. 3, p. 035302, 2015.

[36] T. Fukuhara, A. Kantian, M. Endres, M. Cheneau, P. Schauß, S. Hild, D. Bellem, U. Schollwöck, T. Giamarchi, C. Gross, *et al.*, "Quantum dynamics of a mobile spin impurity," *Nature Physics*, vol. 9, no. 4, pp. 235–241, 2013.

[37] C. Gross and I. Bloch, "Quantum simulations with ultracold atoms in optical lattices," *Science*, vol. 357, no. 6355, pp. 995–1001, 2017.

[38] J. P. Dowling and G. J. Milburn, "Quantum technology: the second quantum revolution," *Philosophical Transactions of the Royal Society of London. Series A: Mathematical, Physical and Engineering Sciences*, vol. 361, no. 1809, pp. 1655–1674, 2003.

[39] L. Aolita, F. de Melo, and L. Davidovich, "Open-system dynamics of entanglement:a key issues review," *Rep. Prog. Phys.*, vol. 78, p. 042001, mar 2015.

[40] P. S. Correia and F. de Melo, "Spin-entanglement wave in a coarse-grained optical lattice," *Physical Review A*, vol. 100, no. 2, p. 022334, 2019.

[41] V. Subrahmanyam, "Entanglement dynamics and quantum-state transport in spin chains," *Physical Review A*, vol. 69, no. 3, p. 034304, 2004.

[42] L. Amico, A. Osterloh, F. Plastina, R. Fazio, and G. M. Palma, "Dynamics of entanglement in one-dimensional spin systems," *Physical Review A*, vol. 69, no. 2, p. 022304, 2004.

[43] I. Bloch, "Ultracold quantum gases in optical lattices," *Nature Physics*, vol. 1, no. 1, pp. 23–30, 2005.

[44] I. Bloch, "Quantum gases in optical lattices," *Physics World*, vol. 17, no. 4, p. 25, 2004.

[45] L.-M. Duan, E. Demler, and M. D. Lukin, "Controlling spin exchange interactions of ultracold atoms in optical lattices," *Physical Review Letters*, vol. 91, no. 9, p. 090402, 2003.

[46] N. Konno, "Limit theorem for continuous-time quantum walk on the line," *Physical Review E*, vol. 72, no. 2, p. 026113, 2005.

[47] T. Yu and J. Eberly, "Evolution from entanglement to decoherence of bipartite mixed" x" states," *Quant. Info. Comp.*, vol. 7, p. 459, 2007.

[48] G. Vidal and R. F. Werner, "Computable measure of entanglement," *Physical Review A*, vol. 65, no. 3, p. 032314, 2002.

[49] P. S. Correia, P. C. Obando, R. O. Vallejos, and F. de Melo, "Macro-to-micro quantum mapping and the emergence of nonlinearity," *arXiv preprint arXiv:2007.14370*, 2020.

[50] S. H. Strogatz, *Nonlinear dynamics and chaos: with applications to physics, biology, chemistry, and engineering*. Westview press, 1994.

[51] J. Bae and L.-C. Kwek, "Quantum state discrimination and its applications," *Journal of Physics A: Mathematical and Theoretical*, vol. 48, no. 8, p. 083001, 2015.

[52] R. Renner, "Security of quantum key distribution," *International Journal of Quantum Information*, vol. 6, no. 01, pp. 1–127, 2008.

[53] R. Canetti, "Universally composable security: A new paradigm for cryptographic protocols," in *Proceedings 42nd IEEE Symposium on Foundations of Computer Science*, pp. 136–145, IEEE, 2001.

[54] C. W. Helstrom, "Quantum detection and estimation theory," *J. Stat. Phys.*, vol. 1, no. 2, pp. 231–252, 1969.

[55] M. M. Wolf, "Quantum channels & operations: Guided tour," 2012.

[56] P. Pechukas, "Reduced dynamics need not be completely positive," *Physical review letters*, vol. 73, no. 8, p. 1060, 1994.

[57] A. Shaji and E. Sudarshan, "Who's afraid of not completely positive maps?," *Physics Letters A*, vol. 341, no. 1-4, pp. 48–54, 2005.

[58] F. Iemini, A. Russomanno, D. Rossini, A. Scardicchio, and R. Fazio, "Signatures of many-body localization in the dynamics of two-site entanglement," *Phys. Rev. B*, vol. 94, p. 214206, Dec 2016.

[59] J. Wang, X.-J. Liu, and H. Hu, "Time evolution of quantum entanglement of an EPR pair in a localized environment," *New Journal of Physics*, vol. 20, p. 053015, may 2018.

[60] H.-J. Stöckmann, "Quantum chaos: an introduction," 2000.

[61] E. Fiordilino, "The emergence of chaos in quantum mechanics," *Symmetry*, vol. 12, no. 5, p. 785, 2020.

Appendix A

Evaluation of the average state

A.1 Averaging assignment: open quantum system

Here we explicitly evaluate the average state related to the partial trace case, in equation (4.5). The method to be presented here will serve as inspiration for the calculation of the average state related to the blurred and saturated detector.

Given the partial trace map $\mathrm{tr}_E : \mathcal{L}(\mathcal{H}_S \otimes \mathcal{H}_E) \to \mathcal{L}(\mathcal{H}_S)$ and a coarse-grained description $\varrho \in \mathcal{L}(\mathcal{H}_S)$, the average state $\mathcal{A}_{\mathrm{tr}_E}[\varrho]$ is given by

$$\mathcal{A}_{\mathrm{tr}_E}[\varrho] = \int d\mu_\psi \mathrm{Pr}_{\mathrm{tr}_E}(\psi|\varrho)\psi; \tag{A.1}$$

where $d\mu_\psi$ is the uniform Haar measure in $\mathcal{H}_S \otimes \mathcal{H}_E$, and the conditional probability $\mathrm{Pr}_{\mathrm{tr}_E}(\psi|\varrho)$ is non-null only in $\Omega_{\mathrm{tr}_E}(\varrho) = \{|\psi\rangle \in \mathcal{H}_S \otimes \mathcal{H}_E \,|\, \mathrm{tr}_E[|\psi\rangle\langle\psi|] = \varrho\}$. The elements of $\Omega_{\mathrm{tr}_E}(\varrho)$ are thus the purifications of ϱ in the extended space $\mathcal{H}_S \otimes \mathcal{H}_E$.

In order to abide by the coarse-graining constraint, the conditional probability distribution $\mathrm{Pr}_{\mathrm{tr}_E}(\psi|\varrho)$ must be proportional to $\delta(\mathrm{tr}_E[\psi] - \varrho)$. Such a probability is invariant by unitary transformations in the "environment" part, that is:

$$\mathrm{Pr}_{\mathrm{tr}_E}(\psi|\varrho) = \mathrm{Pr}_{\mathrm{tr}_E}(\mathbb{1}\otimes U\psi\mathbb{1}\otimes U^\dagger|\varrho),\ \forall U \in \mathcal{L}(\mathcal{H}_E). \tag{A.2}$$

As the purifications of ϱ are connected by local unitary transformations acting in $\mathcal{H}_E$,

this invariance implies that all the elements in $\Omega_{\mathrm{tr}_E}(\varrho)$, given no further constraints, are equally likely.

Since the Haar measure $d\mu_\psi$ is also invariant by unitary transformations, the average state for the partial trace case can be equivalently written by changing the variables $|\psi\rangle \to \mathbb{1}\otimes U|\psi\rangle$ as:

$$\mathcal{A}_{\mathrm{tr}_E}[\varrho] = \int d\mu_\psi \mathrm{Pr}_{\mathrm{tr}_E}(\psi|\varrho)\, \mathbb{1}\otimes U\psi\mathbb{1}\otimes U^\dagger. \tag{A.3}$$

Given the choice of unitary U in the equation above plays no role, we can average over all such unitary transformations, to obtain:

$$\mathcal{A}_{\mathrm{tr}_E}[\varrho] = \int d\mu_\psi \mathrm{Pr}_{\mathrm{tr}_E}(\psi|\varrho)\, \overline{\mathbb{1}\otimes U\psi\mathbb{1}\otimes U^\dagger}^{\mu_U}. \tag{A.4}$$

As we have established an equal probability for all states in $\Omega_{\mathrm{tr}_E}(\varrho)$, this average is performed using the Haar measure on the environment part, and its explicit evaluation is a standard result in quantum information [55]:

$$\overline{\mathbb{1}\otimes U\psi\mathbb{1}\otimes U^\dagger}^{\mu_U} = \mathrm{tr}_E[\psi]\otimes\frac{\mathbb{1}}{d_E} = \varrho\otimes\frac{\mathbb{1}}{d_E}. \tag{A.5}$$

Note that the above result is independent of ψ, depending only on the coarse-grained density matrix ϱ. The integral in (A.4) is then now easily calculated:

$$\begin{aligned}\mathcal{A}_{\mathrm{tr}_E}[\varrho] &= \varrho\otimes\frac{\mathbb{1}}{d_E}\overbrace{\int d\mu_\psi\, \mathrm{Pr}_{\mathrm{tr}_E}(\psi|\varrho)}^{=1}\\ &= \varrho\otimes\frac{\mathbb{1}}{d_E}.\end{aligned} \tag{A.6}$$

Therefore, in the partial trace case, the average state is just the tensor product between the coarse-grained state ϱ and the identity in subspace $\mathcal{H}_E$.

A.2 Averaging assignment: blurred and saturated detector

Here we calculate the average state related to the blurred and saturated detector, as induced by the coarse-graining map $\Lambda_{\text{BnS}} : \mathcal{L}(\mathcal{H}_4) \to \mathcal{L}(\mathcal{H}_2)$, in equation (4.8). Following the same steps as in the above calculation, the average assignment for the present case is given by:

$$\mathcal{A}_{\Lambda_{\text{BnS}}}[\varrho] = \int d\mu_\psi \text{Pr}_{\Lambda_{\text{BnS}}}(\psi|\varrho)\psi; \tag{A.7}$$

where $d\mu_\psi$ is the uniform Haar measure in $\mathcal{H}_4$, and the conditional probability distribution $\text{Pr}_{\Lambda_{\text{BnS}}}(\psi|\varrho)$ is non-null only in $\Omega_{\Lambda_{\text{BnS}}}(\varrho) = \{|\psi\rangle \in \mathcal{H}_4 \,|\, \Lambda_{\text{BnS}}[|\psi\rangle\langle\psi|] = \varrho\}$.

The coarse-graining constraints imply that $\text{Pr}_{\Lambda_{\text{BnS}}}(\psi|\varrho) \propto \delta(\Lambda_{\text{BnS}}[|\psi\rangle\langle\psi|] - \varrho)$. Here, however, the symmetry obeyed by this conditional probability distribution is not so immediately spotted. In order to make it apparent, we write $|\psi\rangle$ in the computational basis in $\mathcal{H}_4$ as $|\psi\rangle = \sum_{i,j=0}^{1} c_{ij}|ij\rangle$, where $c_{ij} \in \mathbb{C}$, and $\sum_{ij} |c_{ij}|^2 = 1$. Consequently, the average assignment can be written as:

$$\mathcal{A}_{\Lambda_{\text{BnS}}}[\varrho] = \int dc_{00}dc_{01}dc_{10}dc_{11}\text{Pr}_{\Lambda_{\text{BnS}}}(c_{00}, c_{01}, c_{10}, c_{11}|\varrho)\, \psi(c_{00}, c_{01}, c_{10}, c_{11})\times \\ \times\, \delta(|c_{00}|^2 + |c_{01}|^2 + |c_{10}|^2 + |c_{11}|^2 - 1). \tag{A.8}$$

Now note that the action of Λ_{BnS} on ψ is the following one:

$$\Lambda_{\text{BnS}}[\psi] = \begin{pmatrix} |c_{00}|^2 & \frac{1}{\sqrt{3}}c_{00}[c_{01}^* + c_{10}^* + c_{11}^*] \\ \frac{1}{\sqrt{3}}c_{00}^*[c_{01} + c_{10} + c_{11}] & |c_{01}|^2 + |c_{10}|^2 + |c_{11}|^2 \end{pmatrix}. \tag{A.9}$$

Therefore, in terms of the coefficients c_{ij}, the proportionality $\Pr_{\Lambda_{\text{BnS}}}(\psi|\varrho) \propto \delta(\Lambda_{\text{BnS}}[|\psi\rangle\langle\psi|] - \varrho)$ can be rewritten as:

$$\Pr_{\Lambda_{\text{BnS}}}(c_{00}, c_{01}, c_{10}, c_{11}|\varrho) \propto \delta\big(|c_{00}|^2 - \varrho_{00}\big) \times \tag{A.10}$$

$$\times\, \delta\big(|c_{01}|^2 + |c_{10}|^2 + |c_{11}|^2 - \varrho_{11}\big) \times \tag{A.11}$$

$$\times\, \delta\Big(\frac{c_{00}}{\sqrt{3}}[c_{01}^* + c_{10}^* + c_{11}^*] - \varrho_{01}\Big), \tag{A.12}$$

where $\varrho_{ij} = \langle i|\varrho|j\rangle$ are the components of ϱ in the computational basis in $\mathcal{H}_2$. Note that the normalization restriction $\delta(|c_{00}|^2 + |c_{01}|^2 + |c_{10}|^2 + |c_{11}|^2 - 1)$ is already implied by the normalization of ϱ and the constraints in (A.10) and (A.11).

The coefficients c_{ij} are complex numbers, and can be thus be written as $c_{ij} = a_{ij} + \mathrm{i}\, b_{ij}$ with $a_{ij}, b_{ij} \in \mathbb{R}$. In this sense, in order to calculate the integral in (A.8) it is convenient to rewrite $|\psi\rangle$ as:

$$|\psi\rangle = YV, \tag{A.13}$$

with Y and V respectively defined as:

$$Y \equiv \begin{pmatrix} 1 & 0 & 0 & 0 & i & 0 & 0 & 0 \\ 0 & 1 & 0 & 0 & 0 & i & 0 & 0 \\ 0 & 0 & 1 & 0 & 0 & 0 & i & 0 \\ 0 & 0 & 0 & 1 & 0 & 0 & 0 & i \end{pmatrix}, \quad V \equiv \begin{pmatrix} a_{00} \\ a_{01} \\ a_{10} \\ a_{11} \\ b_{00} \\ b_{01} \\ b_{10} \\ b_{11} \end{pmatrix}. \tag{A.14}$$

The density matrix representation is then equivalently written as $|\psi\rangle\langle\psi| = YVV^TY^\dagger$, with the average state (A.8) expressed now as:

$$\mathcal{A}_{\Lambda_{\text{BnS}}}[\varrho] = \int dV \, \Pr_{\Lambda_{\text{BnS}}}(V|\varrho)\, YVV^TY^\dagger\, \delta(V^TV - 1), \tag{A.15}$$

where $dV = \prod_{i,j=0}^{1} da_{ij}db_{ij}$ and the probability

$$\Pr_{\Lambda_{\text{BnS}}}(V|\varrho) \equiv \Pr_{\Lambda_{\text{BnS}}}(a_{00}, \ldots, a_{11}, b_{00}, \ldots, b_{11}|\varrho). \tag{A.16}$$

Without loss of generality we can ignore a global phase and consider c_{00} real, such that $a_{00} = c_{00}$ and $b_{00} = 0$. With these considerations, $\Pr_{\Lambda_{\text{BnS}}}(V|\varrho)$ can be rewritten as the following product of the delta functions:

$$\Pr_{\Lambda_{\text{BnS}}}(V|\varrho) \propto \delta\big(a_{00}^2 - \varrho_{00}\big) \times \delta\big(b_{00}\big) \times \tag{A.17}$$

$$\delta\big(a_{01}^2 + a_{10}^2 + a_{11}^2 + b_{01}^2 + b_{10}^2 + b_{11}^2 - \varrho_{11}\big) \times \tag{A.18}$$

$$\delta\Big(\frac{a_{00}}{\sqrt{3}}(a_{01} + a_{10} + a_{11}) - \mathfrak{Re}[\varrho_{01}]\Big) \times \tag{A.19}$$

$$\delta\Big(-\frac{a_{00}}{\sqrt{3}}(b_{01} + b_{10} + b_{11}) - \mathfrak{Im}[\varrho_{01}]\Big). \tag{A.20}$$

The first two delta functions in the expression above already fix $a_{00} = \sqrt{\varrho_{00}}$, and $b_{00} = 0$. The second line, (A.18), imposes a spherical symmetry for the real coefficients in the excited subspace, as it is equivalent to a sphere of radius $\sqrt{\varrho_{11}}$ in such a subspace. This symmetry suggests the conditional probability $\Pr_{\Lambda_{\text{BnS}}}(V|\varrho)$ to be invariant over orthogonal transformations on the excited subspace.

The orthogonal transformations that leave $\Pr_{\Lambda_{\text{BnS}}}(V|\varrho)$ invariant are, however, further restricted by the constraints in Eqs. (A.19) and (A.20). The allowed transformations are those that maintain the hyper-planes $a_{01} + a_{10} + a_{11} = \sqrt{3}\mathfrak{Re}[\varrho_{01}]/a_{00}$ and $b_{01} + b_{10} + b_{11} = -\sqrt{3}\mathfrak{Im}[\varrho_{01}]/a_{00}$ invariant. Such transformations are rotations in the corresponding subspaces along vectors normal to the hyper-planes.

We thus established that

$$\mathrm{Pr}_{\Lambda_{\mathrm{BnS}}}(V|\varrho) = \mathrm{Pr}_{\Lambda_{\mathrm{BnS}}}(O(\theta,\phi)V|\varrho). \tag{A.21}$$

for orthogonal transformations of the form

$$O(\theta,\phi) = \mathbb{1}\oplus R_a(\theta)\oplus\mathbb{1}\oplus R_b(\phi) = \begin{pmatrix} 1 & 0 & 0 & 0 & 0 & 0 & 0 & 0 \\ 0 & & & & 0 & 0 & 0 & 0 \\ 0 & & R_a(\theta) & & 0 & 0 & 0 & 0 \\ 0 & & & & 0 & 0 & 0 & 0 \\ 0 & 0 & 0 & 0 & 1 & 0 & 0 & 0 \\ 0 & 0 & 0 & 0 & 0 & & & \\ 0 & 0 & 0 & 0 & 0 & & R_b(\phi) & \\ 0 & 0 & 0 & 0 & 0 & & & \end{pmatrix}, \tag{A.22}$$

where $R_a(\theta)$ is a rotation in the "a" excited subspace by an angle $\theta \in [0, 2\pi[$ along the axis $a = (1,1,1)$, and similarly, $R_b(\phi)$ is a rotation in the "b" excited subspace by an angle $\phi \in [0, 2\pi[$ along the axis $b = (1,1,1)$.

Now we can proceed as for the partial trace case. Using the invariance property (A.21) in the average assigned description (A.15) we get:

$$\begin{aligned}\mathcal{A}_{\Lambda_{\mathrm{BnS}}}[\varrho] = &\int d(O(\theta,\phi)V)\ \mathrm{Pr}_{\Lambda_{\mathrm{BnS}}}(O(\theta,\phi)V|\varrho)\, YO(\theta,\phi)VV^TO^T(\theta,\phi)Y^\dagger\times \\ &\times \delta(V^TO^T(\theta,\phi)O(\theta,\phi)V - 1)\end{aligned} \tag{A.23}$$

$$= \int dV\ \mathrm{Pr}_{\Lambda_{\mathrm{BnS}}}(V|\varrho)\, YO(\theta,\phi)VV^TO^T(\theta,\phi)Y^\dagger\delta(V^TV - 1), \tag{A.24}$$

where we used that $d(O(\theta,\phi)V) = dV$ as $O(\theta,\phi)$ is an orthogonal transformation. As the above equation is true for any choice of θ and ϕ, we can uniformly average over these

parameters to get:

$$\mathcal{A}_{\Lambda_{\text{BnS}}}[\varrho] = \int dV \, \Pr_{\Lambda_{\text{BnS}}}(V|\varrho) \, Y \overline{O(\theta,\phi) V V^T O^T(\theta,\phi)}^{\mu_O} Y^\dagger \, \delta(V^T V - 1), \tag{A.25}$$

where μ_O is the uniform measure over the orthogonal transformations $O(\theta,\phi)$. Explicitly, this averaging can be written as:

$$Y \overline{O(\theta,\phi) V V^T O^T(\theta,\phi)}^{\mu_O} Y^\dagger = Y \left(\frac{1}{(2\pi)^2} \int_0^{2\pi} d\theta \int_0^{2\pi} d\phi \, O(\theta,\phi) V V^T O^T(\theta,\phi) \right) Y^\dagger. \tag{A.26}$$

Although tedious, the integral can be exactly calculated, and leads to the following matrix:

$$Y \overline{O(\theta,\phi) V V^T O^T(\theta,\phi)}^{\mu_O} Y^\dagger = \begin{pmatrix} \bigcirc & \triangle & \triangle & \triangle \\ \triangle^* & \Diamond & \square & \square \\ \triangle^* & \square & \Diamond & \square \\ \triangle^* & \square & \square & \Diamond \end{pmatrix}, \tag{A.27}$$

with the coefficients $\bigcirc, \Diamond, \triangle$ and $\square$ dependent of a_{ij} and b_{ij} as follows:

$$\begin{aligned} \bigcirc &= a_{00}^2, \\ \Diamond &= \frac{1}{3}(a_{01}^2 + a_{10}^2 + a_{11}^2 + b_{01}^2 + b_{10}^2 + b_{11}^2), \\ \triangle &= \frac{1}{3} a_{00}(a_{01} + a_{10} + a_{11} - i\, b_{01} - i\, b_{10} - i\, b_{11}), \\ \square &= \frac{1}{3}(a_{01}a_{10} + a_{01}a_{11} + a_{10}a_{11} + b_{01}b_{10} + b_{01}b_{11} + b_{10}b_{11}). \end{aligned} \tag{A.28}$$

Employing the constraints in Eqs.(A.17) - (A.20), these coefficients can be rewritten as

$$\bigcirc = \varrho_{00}, \qquad \Diamond = \frac{\varrho_{11}}{3}, \qquad \triangle = \frac{\varrho_{01}}{\sqrt{3}}, \qquad \square = \frac{3|\triangle|^2}{\bigcirc} - \frac{\Diamond}{2}. \tag{A.29}$$

With these results, we finally get:

$$Y\overline{O(\theta,\phi)VV^TO^T(\theta,\phi)}^{\mu_O}Y^\dagger = \begin{pmatrix} \varrho_{00} & \frac{\varrho_{01}}{\sqrt{3}} & \frac{\varrho_{01}}{\sqrt{3}} & \frac{\varrho_{01}}{\sqrt{3}} \\ \frac{\varrho_{01}^*}{\sqrt{3}} & \frac{\varrho_{11}}{3} & \frac{|\varrho_{01}|^2}{2\varrho_{00}} - \frac{\varrho_{11}}{6} & \frac{|\varrho_{01}|^2}{2\varrho_{00}} - \frac{\varrho_{11}}{6} \\ \frac{\varrho_{01}^*}{\sqrt{3}} & \frac{|\varrho_{01}|^2}{2\varrho_{00}} - \frac{\varrho_{11}}{6} & \frac{\varrho_{11}}{3} & \frac{|\varrho_{01}|^2}{2\varrho_{00}} - \frac{\varrho_{11}}{6} \\ \frac{\varrho_{01}^*}{\sqrt{3}} & \frac{|\varrho_{01}|^2}{2\varrho_{00}} - \frac{\varrho_{11}}{6} & \frac{|\varrho_{01}|^2}{2\varrho_{00}} - \frac{\varrho_{11}}{6} & \frac{\varrho_{11}}{3} \end{pmatrix}. \tag{A.30}$$

Note that the above matrix is independent of V, i.e., it is independent of $|\psi\rangle$, depending only on the elements of the effective given state ϱ. As such, the average assignment can be obtained as:

$$\begin{aligned} \mathcal{A}_{\Lambda_{\text{BnS}}}[\varrho] &= Y\overline{O(\theta,\phi)VV^TO^T(\theta,\phi)}^{\mu_O}Y^\dagger \overbrace{\int dV\ \Pr_{\Lambda_{\text{BnS}}}(V|\varrho)\delta(V^TV-1)}^{=1} \\ &= Y\overline{O(\theta,\phi)VV^TO^T(\theta,\phi)}^{\mu_O}Y^\dagger. \end{aligned} \tag{A.31}$$

Thus the average state related to the blurred and saturated coarse-graining is given by (A.30).